

1 **Impact of physical processes on the phytoplankton blooms**  
2 **in the South China Sea: An eddy-resolving**  
3 **physical-biological model study**

4

5 **Y.Sasai<sup>1</sup>, H. Sasaki<sup>2</sup>, and K.J.Richards<sup>3</sup>**

6 [1]{Research Institute for Global change, Japan Agency for Marine-Earth Science and  
7 Technology, Yokohama, Japan}

8 [2]{Earth Simulator Center, Japan Agency for Marine-Earth Science and Technology,  
9 Yokohama, Japan}

10 [3]{International Pacific Research Center, SOEST, University of Hawaii, Honolulu, USA}

11 Correspondence to: Y.Sasai ([ysasai@jamstec.go.jp](mailto:ysasai@jamstec.go.jp))

12

13 **Abstract**

14 An eddy-resolving coupled physical-biological ocean model has been employed to investigate  
15 the physical influences on phytoplankton blooms in the South China Sea during 2000-2007.  
16 The model captures the seasonal and interannual variability of surface chlorophyll distribution  
17 associated with mesoscale eddies, ocean circulation and upwelling generated by the monsoon  
18 winds. The model also reproduces the high chlorophyll distributions in two coastal upwelling  
19 regions: the northwestern Luzon in winter and the eastern coast of Vietnam in summer. To the  
20 northwest of Luzon, the monsoon driven-upwelling, anticyclonic eddies, and the intrusion of  
21 the Kuroshio has a large impact on the winter phytoplankton bloom. The model shows the  
22 winter phytoplankton bloom is induced by the shallow nutricline depth under the northeast  
23 monsoon. Strong vertical motions at the edge of anticyclonic eddy enhance the phytoplankton  
24 bloom and produce the filamentary structure. Off the eastern coast of Vietnam, the  
25 monsoon-driven upwelling and anticyclonic circulation control the high chlorophyll  
26 distribution in summer. During the southwest monsoon, strong offshore Ekman transport and  
27 upwelling occur and increase the surface chlorophyll. The high chlorophyll is advected from  
28 the coast to open ocean by the strong offshore circulation.

29

## 1 **1 Introduction**

2 The South China Sea (SCS) is influenced strongly by the monsoon system. The seasonal  
3 variation of monsoonal winds drives the surface oceanic circulation and upwelling in this  
4 region (e.g., Wyrski, 1961; Shaw and Chao, 1994; Liu and Xie, 1999; Liu et al., 2002). The  
5 alternating monsoons in summer and winter lead to changes in the upper circulation system.  
6 In summer, the strong southwesterly winds drive an anticyclonic gyre in the SCS and result in  
7 localized upwelling off Vietnam (e.g., Kuo et al., 2000; Liu et al., 2002; Xie et al., 2003). In  
8 winter, the northeasterly winds force a cyclonic gyre in the SCS and drive the localized  
9 upwelling off the western Luzon (e.g., Qu, 2000; Liu et al., 2002).

10 The seasonal variation of the chlorophyll distribution in the SCS is very much affected by the  
11 alternating monsoon winds and resultant changes in ocean circulation. The strong upwelling  
12 induced by the monsoon contributes to the high chlorophyll concentrations found in the areas  
13 off eastern Vietnam, and off western Luzon. During the southwest monsoon (May to  
14 September), the surface chlorophyll maximum occurs off the east coast of Vietnam. During  
15 the northeast monsoon (November to March), blooms appear off the northwest coast of Luzon,  
16 and the surface chlorophyll concentration in the upwelling regions is much reduced. Tang et  
17 al. (1999, 2004) investigated the effects of wind forcing on the phytoplankton blooms off the  
18 northwest of Luzon and off the east coast of Vietnam using hydrographic and satellite data.  
19 They indicated the phytoplankton blooms were related to upwelling, which brings nutrients to  
20 the surface waters. Wang et al. (2010) indicated that the winter phytoplankton bloom off the  
21 northwest of Luzon is primarily induced by both Ekman pumping-driven upwelling and upper  
22 mixed layer entrainment. In addition to the seasonal variation, the SCS circulation also shows  
23 the interannual variability related to the El Niño Southern Oscillation (e.g., Kuo et al., 2004;  
24 Liu et al., 2004; Fang et al., 2006) and Indian Ocean Dipole (IOD) (Saji et al., 1999; Yang et  
25 al., 2010) the latter having a considerable impact on the southwest monsoon over the SCS.

26 Mesoscale eddies are an important component of ocean dynamics in the SCS (Wang et al.,  
27 2003; Liu et al., 2008; Chen et al., 2011). They play an important role in the transport of heat,  
28 salt and biogeochemical tracers. Eddies affect the rates of nutrient supply to the euphotic zone  
29 through upwelling and downwelling, with a resultant change in phytoplankton productivity.  
30 To investigate the physical characters of mesoscale eddies in the SCS, many studies have  
31 been performed (e.g., Chi et al., 1998; Wang et al., 2003; Xiu et al., 2010; Zhuang et al.,  
32 2010). However, only limited studies, based on a few cruises data and satellite data, have

1 focused on the impact of eddy activity on the phytoplankton productivity. Ning et al. (2004)  
2 observed high chlorophyll and primary production in cyclonic eddies and low chlorophyll and  
3 primary production in anticyclonic eddies. Chen et al. (2007) observed enhanced primary  
4 production in a cyclonic eddy in Luzon Strait. Lin et al. (2010) studied the phytoplankton  
5 bloom produced by an anticyclonic eddy injection in the oligotrophic area of the northern  
6 SCS. These studies, based on shipboard measurements, are limited both in time and space.

7 The physical-biological model provides a useful tool to address questions concerning the role  
8 of physical processes and their impact on the biogeochemical processes at different scales.  
9 Liu et al. (2002) demonstrated that the uplifted nutricline in association with the monsoon  
10 winds generated the observed level of chlorophyll in the SCS. They also simulated the high  
11 chlorophyll concentration off the east coast of Vietnam during the southwest monsoon and off  
12 the northwest of Luzon during the northeast monsoon. Liu and Chai (2009) investigated the  
13 seasonal and interannual variations of biogeochemical processes in the SCS. They showed the  
14 interannual variation of biological productivity is weaker than the seasonal variation. Xiu and  
15 Chai (2011) focused on the biogeochemical response to the modeled mesoscale eddies in the  
16 SCS. They compared the chlorophyll and new production in the cyclonic and anticyclonic  
17 eddies with the SCS basin mean. They showed cyclonic eddies enhance the chlorophyll and  
18 new production, and anticyclonic eddies reduce them.

19 In this study, we focus on the effect of monsoon variation and eddy activity on the  
20 phytoplankton blooms in the SCS using output of an eddy-resolving ( $0.1^\circ$ ) global  
21 physical-biological model (Sasai et al., 2006, 2010). The eddy-resolving model captures  
22 mesoscale phenomena such as narrow boundary currents, filamentary structures, coastal  
23 upwelling, and eddy variability. We determine the seasonal variability of phytoplankton  
24 blooms influenced by the several scales of variability of physical processes and also examine  
25 the spatial response of phytoplankton blooms to interannual scale variability during the  
26 2000-2007 period.

27

## 28 **2 Model Description**

29 The physical model is the Ocean general circulation model For the Earth Simulator (OFES)  
30 (Masumoto et al., 2004), which is based on the Geophysical Fluid Dynamics Laboratory's  
31 Modular Ocean Model (MOM3) (Pacanowski, and Griffies, 2000). The model domain covers  
32 a near global region, except for the Arctic Ocean, extending from  $75^\circ\text{S}$  to  $75^\circ\text{N}$ . The

1 horizontal resolution is  $0.1^\circ$ . There are 54 vertical levels, with varying thickness between the  
2 levels from 5 m at the surface to 330 m at the maximum depth of 6065 m. The model  
3 topography is constructed from the  $1/30^\circ$  bathymetry dataset created by the OCCAM Project  
4 at the Southampton Oceanography Center. After the physical fields have been spun up for 50  
5 years under the climatological monthly mean data of NCEP/NCAR, the OFES is forced by  
6 the daily mean NCEP/NCAR reanalysis data (Kalnay et al., 1996) for 48 years from 1950 to  
7 1998. The last day of 1998 is used for the initial physical fields for this simulation.

8 The marine ecosystem model is a simple nitrogen-based four-compartment, NPZD (Nitrate,  
9 Phytoplankton, Zooplankton and Detritus), ecosystem model (Oschlies, 2001). The evolution  
10 of the biological tracer concentrations in the OFES is governed by an advection-diffusion  
11 equation with source and sink terms. The source and sink terms represent the biological  
12 processes (Sasai et al., 2006,2010). The biological processes include phytoplankton growth,  
13 zooplankton grazing, mortality, and detritus remineralization. The ecosystem model is  
14 described in Appendix A. The initial nitrate field is taken from the climatological dataset  
15 (WOA98) and has no supply from the atmosphere and rivers. The initial P and Z  
16 concentrations are set to  $0.14 \text{ mmol m}^{-3}$  and  $0.014 \text{ mmol m}^{-3}$  at the surface, respectively,  
17 decreasing exponentially with a scale depth of 100 m (Sarmiento *et al.* 1993). D is initialized  
18 to  $10^{-4} \text{ mmol m}^{-3}$  everywhere. To establish a stable pattern of the biological fields, the  
19 biological model is incorporated after the physical field of OFES is spun up for 50 years  
20 under the climatological monthly mean data. The biological model coupled with the evolving  
21 physical fields is integrated over a 5-year period under the climatological monthly mean data  
22 (Sasai et al., 2006). The variability of biological fields has no feedback on the physical fields.  
23 The biological fields at the end of coupled 5-year integration are used as initial conditions for  
24 biological fields for this simulation.

25 For the experiment reported here, the coupled physical-biological model (OFES-NPZD) is  
26 forced by the daily mean surface wind stress data of Quick Scatterometer (QSCAT) and  
27 atmospheric daily mean data (heat and salinity fluxes) of the NCEP/NCAR reanalysis from  
28 1999 to 2007. We use OFES-NPZD outputs for the SCS domain. Results are presented for  
29 years 2000 to 2007. The simulated phytoplankton concentration ( $\text{mmol N m}^{-3}$ ) is converted to  
30 chlorophyll concentration ( $\text{mg m}^{-3}$ ) using a ratio of 1.59 g chlorophyll per mol nitrogen  
31 (Cloern et al., 1995; Oschlies, 2001). To investigate the performance of the coupled  
32 physical-biological model, we compare our results with the ocean color satellite image data of

1 the Sea-viewing Wide Field-of-View Sensor (SeaWiFS).

2

### 3 **3 Results**

#### 4 **3.1 Seasonal variability of physical and biological fields**

5 Ocean color satellite images reveal two seasons (summer and winter) of the surface  
6 chlorophyll distribution in the South China Sea, especially, off the east coast of Vietnam and  
7 off the northwestern Luzon (Fig. 1). Fig. 1 also shows the peak conditions of the model  
8 surface chlorophyll, the vertical mean nitrate concentration over the upper 73 m depth, the  
9 thermocline depth, and vertical nitrate flux at 73 m depth during the summer (August) and  
10 winter (December) monsoons. The 73 m depth is close to the subsurface chlorophyll  
11 maximum depth in the model. In August, SeaWiFS shows a band of high chlorophyll  
12 concentration ( $> 0.3 \text{ mg m}^{-3}$ ) about 100 km wide extending 500 km northwestward off the  
13 east coast of Vietnam. High chlorophyll concentration also appears along the coast of  
14 southwestern China, and the south of Vietnam. The simulated chlorophyll distribution  
15 represents same pattern of the SeaWiFS off the east coast of Vietnam, but has a relatively low  
16 concentration along the coast of southwestern China and the south coast of Vietnam. Off the  
17 east coast of Vietnam, the high chlorophyll ( $> 0.3 \text{ mg m}^{-3}$ ) area extends about 100 km wide  
18 from the coast to the open ocean (500 km). The high chlorophyll concentration region is  
19 strongly related to the southwesterly monsoon wind. The southwesterly winds produce coastal  
20 upwelling (upward Ekman pumping) off the east coast of Vietnam and drive the anticyclonic  
21 gyre in the southern basin of SCS. The surface current off the Vietnam is also clearly  
22 reproduced (Figs. 2a and 2b). The coastal upwelling brings cold, nutrient rich close to the  
23 surface. There is large vertical nitrate flux ( $> 4 \text{ mmol N m}^{-2} \text{ d}^{-1}$ ), which induces a  
24 phytoplankton bloom with chlorophyll concentrations in excess of  $0.3 \text{ mg m}^{-3}$ . An offshore  
25 current, which is a part of an anticyclonic gyre, transports the high chlorophyll concentration  
26 from the coast to the open ocean. In the pelagic ocean, excluding the coast and upwelling  
27 regions, the simulated chlorophyll concentration is mostly below  $0.2 \text{ mg m}^{-3}$ , similar to that  
28 seen in SeaWiFS.

29 In December, northeasterly winds are dominant over the SCS, and change the surface  
30 circulation system. The cyclonic circulation is dominant in the SCS basin (Figs. 2a and 2b).  
31 The reversed wind changes the location of the upwelling regions. The upward Ekman

1 pumping area from the southern SCS to the western Luzon inputs high nitrate waters into the  
2 surface layer. The model clearly captures the high chlorophyll ( $> 0.3 \text{ mg m}^{-3}$ ) distribution off  
3 the northwestern Luzon as seen in SeaWiFS data. The high chlorophyll area extends from the  
4 northwestern Luzon to open ocean (500 km). The thermocline depth is shallow ( $< 75 \text{ m}$   
5 depth) and the high nitrate ( $> 1 \text{ mmol N m}^{-3}$ ) waters lift up from the subsurface layer. The  
6 vertical nitrate flux is also strong ( $> 4 \text{ mmol N m}^{-2} \text{ d}^{-1}$ ), and the high surface chlorophyll  
7 conditions are maintained by the nitrate supply from subsurface layer in the northwestern  
8 Luzon. Outside of the coastal and upwelling regions, the simulated chlorophyll concentration  
9 is again below  $0.2 \text{ mg m}^{-3}$ .

10 In general, the seasonal variability of the observed surface chlorophyll distribution is  
11 reproduced in the model. The variability of simulated SSHA is also consistent with the  
12 satellite data, and the gyre circulation pattern in the SCS (e.g., Hu et al., 2000) is well  
13 reproduced. The basin scale pattern of nitrate distribution in summer and winter is similar to  
14 the hydrographic data (Ning et al., 2004). The high nitrate off the east coast of Vietnam in  
15 summer and the high nitrate band in the SCS basin in winter are reproduced. The simulated  
16 nitrate distribution reflects the basin-scale circulation and mesoscale eddies (Fig. 2). In  
17 particular, the model captures the high surface chlorophyll distribution in the coastal  
18 upwelling regions, which is strongly influenced by the monsoon winds, as well as the low  
19 chlorophyll in the open ocean. However, the model underestimates chlorophyll concentrations  
20 along the coast of southwestern China, southern Vietnam, and Philippines Islands. This is  
21 because the coupled physical-biological model does not include nitrate input with river runoff  
22 and benthic nitrate fluxes due to the sedimentary remineralization (Liu et al., 2007).  
23 Additionally, since the parameter values for phytoplankton growth based on open ocean  
24 values, they may not be suitable for the coastal environment (e.g., Liu et al., 2002; Liu and  
25 Chai, 2009). On the other hand, the high value of SeaWiFS data might be unreliable owing to  
26 the high levels of suspended sediments and colored dissolved organic matter (Liu et al.,  
27 2002).

28 To focus on the seasonal variability at two sites strongly affected by changes to the upwelling,  
29 Fig. 3 shows the box-averaged monthly mean surface chlorophyll from observations and  
30 model together with the model isotherm depth, nitrate and nitrate flux, for regions off the  
31 northwestern Luzon and east coast of Vietnam, labeled L and V respectively (see Fig. 1). The  
32 SeaWiFS shows winter phytoplankton blooms off the northwestern Luzon, and high

1 chlorophyll concentrations along the coast of southern Vietnam, southwestern China, and  
2 Philippines Islands in response to the induced upwelling. The wind field is reverse over the  
3 SCS, and the upwelling region is formed in the right of the wind in the northern hemisphere.  
4 The seasonal variability of the simulated surface chlorophyll concentration is similar to that  
5 found in SeaWiFS data for each box (Correlation coefficients are 0.90 in box-L and 0.50 in  
6 box-V, respectively). In Box L, the mean surface chlorophyll concentrations of SeaWiFS and  
7 OFES are  $0.16 \pm 0.07 \text{ mg m}^{-3}$  and  $0.22 \pm 0.10 \text{ mg m}^{-3}$ , respectively. The simulated chlorophyll  
8 concentration is higher than that observed by SeaWiFS. The peak in the simulated surface  
9 chlorophyll concentration ( $0.4 \text{ mg m}^{-3}$ ) in December/January is almost consistent with the  
10 shallow thermocline depth (70 m), the high nitrate concentration ( $> 0.5 \text{ mmol N m}^{-3}$ ) in the  
11 upper 73 meters, and the strong vertical nitrate flux ( $> 0.5 \text{ mmol N m}^{-2} \text{ d}^{-1}$ ). However, the  
12 peak of surface chlorophyll concentration and the peak of vertical mean nitrate concentration  
13 are not synchronous. The peak of surface nitrate concentration appears in December/January  
14 when the MLD is deep and there is a strong vertical nitrate flux, but the peak of subsurface  
15 nitrate concentration appears in February when the nutricline depth is shallow. In Box V, the  
16 mean surface chlorophyll concentrations of SeaWiFS and OFES are  $0.16 \pm 0.04 \text{ mg m}^{-3}$  and  
17  $0.21 \pm 0.02 \text{ mg m}^{-3}$ , respectively. The simulated chlorophyll concentration is also higher than  
18 the SeaWiFS. The observed surface chlorophyll concentration shows a peak in August ( $0.2$   
19  $\text{mg m}^{-3}$ ). The model also shows a peak in surface chlorophyll in August at a time of a  
20 shallowing thermocline, a high vertical nitrate flux and associated increased nitrate levels  
21 induced by the monsoon-driven upwelling. Surface nutrient levels become depleted and the  
22 surface chlorophyll reduces despite the continuing elevated levels of the depth-integrated  
23 nitrate. The peak of vertical mean nitrate concentration is in October when the nutricline is  
24 shallow, and is not at the same time as the peak in surface chlorophyll concentration. The  
25 observed surface chlorophyll shows an increase in November and December. This is caused  
26 by two unusually high chlorophyll events occurring at the end of 2005 and 2007, respectively,  
27 which are not captured by the model (see Fig. 4c - the reason for these events is unclear).

28

### 29 **3.2 Interannual variability of chlorophyll in the two upwelling regions**

30 The timing of the mean seasonal variation of surface chlorophyll off northwestern Luzon  
31 (Box L) and the east coast of Vietnam (Box V) is very much influenced by the seasonal  
32 variation of the monsoon winds (Fig. 2). The relative amplitude of the seasonal cycle,

1 compared to interannual variations, at each location is, however, very different. The time  
2 series of monthly mean surface chlorophyll concentrations of SeaWiFS and OFES and wind  
3 stress averaged for Box L and V during 2000-2007 is shown in Fig. 4. In Box L the signal is  
4 dominated by the seasonal cycle with the peak in chlorophyll occurring close to the beginning  
5 and the end of the year. The correlation coefficient between SeaWiFS and OFES is 0.82, and  
6 the average of surface chlorophyll concentration is  $0.16 \pm 0.07 \text{ mg m}^{-3}$  in SeaWiFS and  
7  $0.20 \pm 0.11 \text{ mg m}^{-3}$  in OFES, respectively. There is interannual variability in the strength of the  
8 peak values in both SeaWiFS and OFES. OFES tends to overestimate the peak but it does  
9 capture the observed relatively high peaks around January 2002, 2004 and 2005. The  
10 exception is the observed high peak around January 2006, which is not found in the OFES  
11 time series. The vertical distribution of properties averaged over Box L is shown in Fig. 5.  
12 Again the seasonal cycle dominates with the bloom in chlorophyll occurring at a time when  
13 the thermocline and nutricline are both shallow (the shallowing being consistent with the  
14 positive upward velocity towards the end of the year). The simulated vertical chlorophyll  
15 distribution is consistent with the hydrographic surveys (Chen et al., 2006). The simulated  
16 subsurface maximum in chlorophyll is at 50 – 80 m depth which is very similar to that  
17 observed. A subsurface maximum in chlorophyll lingers for a few months after the surface  
18 bloom because the shallow nutricline depth is in the euphotic layer during spring and summer.  
19 The depth/time plot of chlorophyll also shows the interannual variations in surface  
20 chlorophyll are, in general, representative of the variations with depth. The exception is again  
21 around January 2006. Also shown in Fig. 4 is the monthly averaged wind stress over the  
22 region. There is no obvious correlation between the strength of the upwelling winds preceding  
23 the winter bloom and the strength of the bloom. Instead interannual variability in the  
24 chlorophyll concentration is most affected by eddy variability and the intrusion of Kuroshio  
25 waters into the SCS. This is looked at in detail in Section 3.4.

26 Off the coast of Vietnam (Box V) seasonal variability is less dominant (Fig 4c), although  
27 there is a peak in surface chlorophyll in most years around August (as seen in the seasonal  
28 mean, Fig 3). The correlation coefficient (0.28) of interannual variability is weaker than the  
29 climatological monthly mean (Fig 3). The average of surface chlorophyll concentration is  
30  $0.16 \pm 0.07 \text{ mg m}^{-3}$  in SeaWiFS and  $0.21 \pm 0.03 \text{ mg m}^{-3}$  in OFES, respectively. The exception is  
31 2004 when there is no significant peak in OFES (and a reduced seasonal cycle in SeaWiFS).  
32 Referring to the depth/time plots in Fig. 6, we see there was a much-reduced seasonal  
33 variation in the depth of the thermocline and nutricline during 2004. There was a modest

1 reduction in the strength of the summer monsoon winds (particularly the eastward component  
2 of wind stress; Fig 4d) during 2004, which may account for the reduced bloom. The average  
3 eastward component of wind stress during summer (June, July, and August) in 2004 is  $0.23 \text{ N}$   
4  $\text{m}^{-3}$  and this value is 30-60% of other years ( $0.33 - 0.55 \text{ N m}^{-3}$ ). The nutricline is deeper (60  
5 m) and the vertical nitrate flux at 73 m depth weaker ( $0.34 \text{ mmol N m}^{-2} \text{ d}^{-1}$ ) in 2004 compared  
6 to other years (when the nutricline depth is 40 – 50 m and nitrate flux is  $0.60 - 1.09 \text{ mmol N}$   
7  $\text{m}^{-2} \text{ d}^{-1}$ ). The highest chlorophyll values are found at a subsurface maximum that varies in  
8 depth between 40 - 60m depth (Fig. 6a) in accord with the varying thermocline and nutricline  
9 depths. The peak in the subsurface maximum occurs slightly later in the year (around  
10 September/October) than at the surface, with a reduced variation in 2004 and 2005 (we note  
11 that in the latter case there was a peak in surface chlorophyll). The large peaks seen in the  
12 observations (but not the model) in late 2005 and 2007 have already been noted. The  
13 SeaWiFS captures the relatively high chlorophyll distribution ( $> 1 \text{ mg m}^{-3}$ ) off the east coast  
14 of Vietnam in late 2005 and 2007 (not shown). However, the model shows a low chlorophyll  
15 concentration in the surface layer because the nitrate supply to the surface layer by the mixing  
16 and upwelling is not much different with other years.

17

### 18 **3.3 Mesoscale eddy activities**

19 Mesoscale eddy activity is an important factor in biological production in the upper layer of  
20 SCS. In the SCS numerous mesoscale eddies are found in a line stretching in a  
21 northeast-southwest direction and southwest of Luzon Strait (Wang et al., 2003; Liu et al.,  
22 2008; Chen et al., 2011). In the west of Luzon Strait, eddies are formed by wind stress curl  
23 variation and the Kuroshio intrusion (e.g., Wang et al., 2000; Yang and Liu, 2003), and  
24 propagate southwestward along the continental slope. The east coast of Vietnam also shows  
25 high mesoscale eddy activity. The variability of western boundary current along the coast  
26 favors the generation of eddies (e.g., Gan and Qu, 2008; Chen et al, 2010). The distribution of  
27 anticyclonic and cyclonic eddies generated by OFES and categorized by the SSHA during  
28 2000-2007, is similar to that observed by satellite altimetry (Chen et al., 2011) (Fig.7). Here  
29 we have taken the 20cm and -20cm SSHA contours to denote anticyclonic and cyclonic  
30 eddies, respectively. The diameter of both eddies in the OFES is from 50 km to 300 km and  
31 the lifetime is from one week to about 7 months.

1

## 2 **3.4 Northwestern Luzon**

3 During the northeasterly winds, the nitrate supply by the vertical advection is strong ( $1 \text{ mmol}$   
4  $\text{N m}^{-2} \text{ d}^{-1}$ ) fueling biological production in the upper ocean in Box L (Figs. 1-5). Additionally,  
5 the northwestern Luzon is an area where numerous eddies are formed (Chen et al, 2011). The  
6 OFES reproduces the number of eddies in the northwestern Luzon during the northeast  
7 monsoon (Figs. 2 and 7). Since both physical processes largely influence on the winter  
8 phytoplankton bloom, we examine the physical and biological fields in the northwestern  
9 Luzon during the northwest monsoon. As a case study, we focus on an anticyclonic eddy  
10 passing through the winter phytoplankton bloom region in OFES. The eddy separated from  
11 the Kuroshio in October 2003 in the Luzon Strait and traveled southwestward along the  
12 continental slope over seven months. The eddy was standing off the northwestern Luzon  
13 during winter.

14 Fig. 8 shows the physical and biological fields in the northern SCS from November 2003 to  
15 February 2004. In this period, the separated anticyclonic eddy (high SSHA in Fig. 8a) from  
16 the Kuroshio has a large effect on the phytoplankton bloom. In the northern SCS, the  
17 intrusion of the Kuroshio as an anticyclonic current loop frequently occurs in the winter (e.g.,  
18 Hu et al., 2000; Qu et al., 2000). A warm-core, anticyclonic eddy from the Kuroshio is also  
19 observed (Li et al., 1998). In October 2003 (not shown), the model anticyclonic eddy is  
20 separated from the Kuroshio in the Luzon Strait. After being separated from the Kuroshio, the  
21 anticyclonic eddy moves from Luzon Strait to the east coast of Vietnam along the continental  
22 slope at an average speed of  $6.0 \text{ cm s}^{-1}$ . The surface current speed of the eddy is about  $1 \text{ m s}^{-1}$ .  
23 The lifetime is about 7 months and the diameter is about 200-300 km. From November 2003  
24 to February 2004, the surface chlorophyll concentration is small ( $< 0.1 \text{ mg m}^{-3}$ ) in the center  
25 of the anticyclonic eddy and is high ( $> 0.2 \text{ mg m}^{-3}$ ) at the edge of eddy, especially, on the  
26 southern side ( $> 0.6 \text{ mg m}^{-3}$ ). On the western side of Luzon (south of the anticyclonic eddy),  
27 the thermocline and nutricline are shallow because of the strong northwesterly winds. In the  
28 center of the anticyclonic eddy, the nitrate concentration remains at a low level ( $< 0.1 \text{ mmol}$   
29  $\text{N m}^{-3}$ ). When the eddy arrives in the high nitrate area, the high nitrate water is drawn out  
30 along the southern edge of the eddy. A filament of high chlorophyll concentration is stretched  
31 out along the south edge of anticyclonic eddy associated with the high nitrate water. There are  
32 large upward and downward motions associated with the eddy.

1 Fig. 9 shows the vertical distribution of chlorophyll concentration, nitrate concentration with  
2 potential density, and vertical velocity along the center of anticyclonic eddy (dashed line in  
3 Fig. 8d). In November 2003, high chlorophyll concentrations ( $> 0.4 \text{ mg m}^{-3}$ ) occur in the  
4 subsurface layer (50 – 75m depth) at the south edge ( $20^{\circ}\text{N}$ ) of the anticyclonic eddy. Potential  
5 density and nutrient contours are pushed down by the presence of the eddy such that at the  
6 center of the eddy low nitrate ( $< 0.1 \text{ mmol N m}^{-3}$ ) water reaches down to 150 m depth. In  
7 December 2003, the chlorophyll concentration in the south edge of anticyclonic eddy  
8 increases ( $> 0.6 \text{ mg m}^{-3}$ ) because the high nitrate water is uplifted along the steep slope of  
9 potential density ( $20^{\circ}\text{N}$ ) by the strong upward vertical velocity ( $> 10 \text{ m day}^{-1}$ ) induced by the  
10 eddy. In January 2004, the slope of potential density surfaces is increased, and the high nitrate  
11 water is brought close to the surface layer. A narrow filament shape of high chlorophyll is  
12 formed at the south edge of anticyclonic eddy ( $19^{\circ}\text{N}$ ). In February 2004, the high nitrate water  
13 ( $> 2.0 \text{ mmol N m}^{-3}$ ) reaches the surface and the chlorophyll concentration is over  $1.5 \text{ mg m}^{-3}$   
14 at the south edge of eddy.

15 In the period 2000-2007, the model captures two incidences (in 2003-2004 and 2004-2005) of  
16 the separated anticyclonic eddy from the Kuroshio passing through the region during the  
17 winter (December-February) phytoplankton bloom in the northern SCS. By overlapping with  
18 the bloom season, the steep slope of potential density with the vertical velocity enhances the  
19 chlorophyll concentration in the south edge of anticyclonic eddy and the areal average of  
20 surface chlorophyll in Box L (Fig. 4a). When the eddy passes through the northern SCS  
21 before or after phytoplankton bloom (as in 2000-2001, 2002-2003), the influence of the eddy  
22 on the phytoplankton bloom is small and the areal average of surface chlorophyll in Box L is  
23 relatively small (Fig 4a). In the case when an eddy passes before the phytoplankton bloom,  
24 the nutricline depth is deep before northeasterly monsoon winds, and at the edge of eddy, the  
25 nitrate supply to the surface is small. In the case when an eddy passes after the phytoplankton  
26 bloom, the nutricline depth is deepening. The nitrate supply by the eddy is again small. In  
27 winters with no detached eddy (2001-2002, 2005-2006, 2006-2007), the intrusion of the  
28 Kuroshio can still impact the chlorophyll concentration along its southern edge (in a manner  
29 similar to that of the detached anticyclonic eddy). Fig. 10 shows the surface chlorophyll  
30 concentration with the horizontal velocity field when the intrusion of Kuroshio occurs in  
31 winter. Along the Kuroshio's southern edge, the phytoplankton bloom is enhanced in all cases.  
32 The impact in 2001-2002 was particularly strong (Fig. 4a).

1

## 2 **3.5 Vietnam coast**

3 Off the east coast of Vietnam, the pattern of the phytoplankton bloom during the southwest  
4 monsoon (July-August) is largely influenced by the coastal upwelling and offshore advection  
5 by an anticyclonic circulation. The OFES reproduces a similar pattern in surface chlorophyll  
6 during this period to that observed by satellites (Tang et al., 2004). Fig. 11 shows the  
7 variability of physical and biological fields from June 2002 to September 2002, which is  
8 typical of most years in the OFES (strongest southwesterly wind in Fig. 4d). The SSHA and  
9 surface horizontal velocity fields show the presence of a strong anticyclonic gyre off the east  
10 coast of Vietnam (Fig. 11a). In June 2002, the current along the east coast of Vietnam is  
11 northward. The chlorophyll concentration near the east coast of Vietnam at around 12°N is  
12 high associated with the high nitrate supply by the shallow nutricline depth and upwelling.  
13 From July 2002 to September 2002, the anticyclonic gyre is dominant during the  
14 southwesterly monsoon winds. The coastal jet separates from the Vietnam coast at around  
15 12°N and flows to the northeast. To the north of the anticyclonic gyre, there is a general  
16 increase in the nitrate concentration at 73m depth (associated with a shallowing thermocline  
17 and nutricline), but note that the higher chlorophyll levels are restricted to the northern edge  
18 of the anticyclonic circulation. Within the anticyclonic gyre, the thermocline and nutricline  
19 are depressed and the nitrate concentration is low ( $< 0.1 \text{ mmol N m}^{-3}$ ). The surface  
20 chlorophyll concentration remains low ( $< 0.2 \text{ mg m}^{-3}$ ).

21 Fig. 12 shows the vertical distribution of chlorophyll concentration, nitrate concentration with  
22 potential density, and vertical velocity across the anticyclonic gyre along 111°E. Associated  
23 with the variation of anticyclonic gyre, the pattern of surface chlorophyll is changed. In June  
24 2002, a subsurface maximum in chlorophyll (50 – 75m depth) appears in the northern side of  
25 anticyclonic gyre (12°N – 15°N) and continues through September. This is in response to the  
26 shallowing thermocline and nutricline north of 12°N. In July 2002, the high chlorophyll  
27 concentration ( $> 0.6 \text{ mg m}^{-3}$ ) is brought to the surface at the northern edge of anticyclonic  
28 circulation (11°N - 13°N). In August 2002, the slope of the potential density surfaces is  
29 increased by the strengthening of the anticyclonic circulation and there is a strong upward  
30 motion ( $> 10 \text{ m day}^{-1}$ ) (Fig. 11d). By September 2002, the current is straight flowing from the  
31 west (coast) to east (open ocean) around 11°N. The chlorophyll concentration at the northern  
32 edge of the anticyclonic circulation (11°N) is decreased because the reduced nitrate supply to

1 the surface layer, but the subsurface chlorophyll maximum layer (around 50 m depth) to the  
2 north of 11°N is maintained, together with the shallow thermocline and nutricline.

3 In the model, the interannual variability of surface chlorophyll distribution off the east coast  
4 of Vietnam is small. The model reproduces the anticyclonic gyre during summer monsoon  
5 (July – August) and the interannual variation is small in the period 2000-2007. The reason for  
6 the small variation of physical fields (circulation pattern and upwelling system) off the east  
7 coast of Vietnam may be the small interannual variability of wind stress field (Fig.4d).

8

#### 9 **4 Conclusions**

10 Climatic variation in the upper ocean of the SCS is primarily controlled by the monsoon. We  
11 have investigated the impact of this variation on the phytoplankton blooms using an  
12 eddy-resolving physical-biological model. For the period from 2000 to 2007, the model  
13 clearly reproduces the seasonal cycle of surface chlorophyll concentration, which is caused by  
14 the seasonal variation of physical processes (upwelling and surface ocean circulation drives  
15 by the surface winds, and the thermocline depth). The spatial distribution of surface  
16 chlorophyll concentration is consistent with the distribution of the thermocline depth and  
17 nutricline depth, implying the surface chlorophyll distribution is mainly controlled by the  
18 nitrate supply from the subsurface layer by vertical mixing and upwelling. In particular, the  
19 seasonal variability of surface chlorophyll concentration in the two upwelling regions  
20 (northwestern Luzon, and east coast of Vietnam) is largely influenced by the monsoon winds.  
21 The phytoplankton bloom peaks in two upwelling regions similar to that observed in  
22 SeaWiFS data. The shallowest period of nutricline depth is also consistent with the  
23 phytoplankton bloom peaks. The nitrate supply by the shoaling of nutricline depth mainly  
24 controls the phytoplankton bloom.

25 To the northwest of Luzon, the winter phytoplankton bloom occurs due to nutrients supplied  
26 from the subsurface layer. The strong northeasterly winds blow parallel to the west coast of  
27 Luzon, and strong offshore Ekman transport and upwelling occur. The nutricline depth is  
28 shallowed by the upwelling and high nutrient waters are supplied by the winter mixing for the  
29 phytoplankton blooms. This result indicates the same winter phytoplankton bloom mechanism  
30 investigated using observed data (Chen et al., 2006). In addition to this mechanism, OFES  
31 also shows the role of anticyclonic eddies and the intrusion of the Kuroshio on the winter  
32 phytoplankton bloom. The timing of these events is important. When the anticyclonic eddy

1 separated from the Kuroshio passes over the region during the winter phytoplankton bloom  
2 the overall strength of the bloom is increased as a filamentary structure on the southern edge  
3 of the eddy. Off the east coast of Vietnam the phytoplankton bloom occurs in the boreal  
4 summer. The mechanism of the summer phytoplankton bloom has been described by Tang et  
5 al. (2004) using satellite data and ship measurements. The strong southwesterly winds blow  
6 parallel to coastline and strong offshore Ekman transport and upwelling occur. The upwelled  
7 nutrients support a strong phytoplankton bloom. The phytoplankton bloom is advected  
8 offshore into the SCS by a strong anticyclonic circulation. OFES captures the detailed  
9 nutrient dynamics and phytoplankton bloom in the open ocean during the southwest monsoon.  
10 The interannual variability of chlorophyll off the east coast of Vietnam is not large in the  
11 OFES during 2000-2007. The model fails to capture the two large observed events in  
12 summer/fall 2005, and summer/fall 2007 (Fig.4c). Liu et al. (2012) showed the high  
13 chlorophyll concentration off the east coast of Vietnam is enhanced by the positive IOD of  
14 2007 and the Madden-Julian Oscillation (MJO) events using the satellite data. The simulated  
15 chlorophyll concentration in 2007 is not large because the reproduced upwelling in the OFES  
16 is not much difference from other years (Fig. 6d).

17

## 18 **Acknowledgement**

19 We thank Drs. Yukio Masumoto, Akio Ishida, and Takashi Kagimoto for their collaborations  
20 in extending the OFES model for biological research. The QSCAT product of J-OFURO was  
21 obtained from Prof. Kunio Kutsuwada. Using ocean color satellite data was obtained from Dr.  
22 Kosei Sasaoka. OFES simulations were conducted on the Earth Simulator under support of  
23 JAMSTEC. This work was partly supported by a Grand-in-Aid for Scientific Research  
24 (22106006 and that on Innovative Areas 2205) from MEXT of Japan.

25

26

27

28

29

30

## 1 **Appendix A: Ecosystem model**

2 The marine ecosystem model is a simple nitrogen-based Nitrate, Phytoplankton, Zooplankton,  
3 and Detritus (NPZD) pelagic model [Oschlies 2001]. The evolution of any biological tracer  
4 concentration  $C_i$  in the OFES is governed by an advective-diffusive-reaction equation

$$5 \frac{\partial C_i}{\partial t} = -\nabla \cdot (u C_i) + \nabla \cdot (A \nabla C) + sms(C_i) \quad (A1)$$

7  
8 where the first and second terms on the right-hand side represent advection, and diffusion,  
9 respectively. The velocity vector,  $u$ , is given by OFES and the lateral and vertical diffusion  
10 coefficients,  $A_h$  and  $A_z$  are the same as used for tracer fields in OFES. The last term is the  
11 source-minus-sink term due to biological activity. For the individual biological tracers  
12 (Phytoplankton,  $P$ , Zooplankton,  $Z$ , Detritus,  $D$ , and Nitrate,  $N$ ), the source-minus-sink terms  
13 are given by

$$14 sms(P) = \bar{J}(z, t, N)P - G(P)Z - \mu_p P - \mu_{pp} P^2 \quad (A2)$$

$$15 sms(Z) = \gamma_1 G(P)Z - \gamma_2 Z - \mu_z Z^2 \quad (A3)$$

$$16 sms(D) = (1 - \gamma_1)G(P)Z + \mu_{pp} P^2 + \mu_z Z^2 - \mu_D D - w_s \frac{\partial D}{\partial z} \quad (A4)$$

$$17 sms(N) = \mu_D D + \gamma_2 Z + \mu_p P - \bar{J}(z, t, N)P \quad (A5)$$

18  
19  
20 where  $\bar{J}$  is the daily averaged phytoplankton growth rate as a function of depth  $z$ , time  $t$ ,  
21 and nitrate concentration,  $N$ .  $G$  is the grazing function. Following [Hurtt Armstrong 1996],  
22 the phytoplankton growth rate is taken to be the minimum of light- and nutrient-limited  
23 growth,

$$24 \bar{J}(z, t, N) = \min \left( \bar{J}(z, t), J_{\max} \frac{N}{k_1 + N} \right) \quad (A6)$$

25  
26 where  $\bar{J}(z, t)$  denotes the purely light-limited growth rate averaged over 24 hours, and  $J_{\max}$   
27 is the light-saturated growth.  $\bar{J}(z, t)$  is computed using the analytical method of [Evans  
28 Parslow 1985].

29

1  
2  
3  
4  
5  
6  
7  
8  
9  
10  
11  
12  
13  
14  
15  
16  
17  
18  
19  
20  
21  
22  
23  
24  
25

$$\bar{J}(z,t) = \frac{1}{\tau_{24h}} \int_0^{24h} \frac{1}{z_k - z_{k+1}} \int_{z_{k+1}}^{z_k} J(z,t) dz dt \quad (A7)$$

where

$$J(z,t) = \frac{V_p \alpha I(z,t)}{[V_p^2 + (\alpha I(z,t))^2]^{1/2}} \quad (A8)$$

$$I(z,t) = I(t)_{z=0} e^{(-\int_z^0 k_c P dz)} \quad (A9)$$

$$I(t)_{z=0} = PAR \tau(t) 2 \frac{\tau_{24h}}{\tau_{sun}} shotwave(t) \quad (A10)$$

$$J_{max} = V_p = ab^{cT} \quad (A11)$$

Following Fasham (1995), the grazing of phytoplankton by zooplankton is given by,

$$G(P) = \frac{g \varepsilon P^2}{g + \varepsilon P^2} \quad (A12)$$

The individual biological parameters are listed in Table A1.

## 1   **References**

- 2
- 3   Chen, C.C., Shiah, F.K., Chung, S.W., and Liu, K.K.: Winter phytoplankton blooms in the  
4   shallow mixed layer of the South China Sea enhanced by upwelling, *J. Mar. Systems*, *59*,  
5   97-110, 2006.
- 6   Chen, G., Hou, Y., and Chu, X.: Mesoscale eddies in the South China Sea: Mean properties,  
7   spatiotemporal variability, and impact on thermocline structure, *J. Geophys. Res.*, *116*,  
8   C06018, doi:10.1029/2010JC006716, 2011.
- 9   Chen, G., Hou, Y., Zhang, Q., and Chu, X.: The eddy pair of eastern Vietnam: Interannual  
10   variability and impact on thermocline structure, *Cont. Shelf Res.*, *30(7)*, 715-723,  
11   doi:10.1016/j.csr.2009.11.013, 2010.
- 12   Chen, Y.-L., Chen, H.-Y., Lin, I.-I., Lee, M.-A., and Chang, J.: Effects of cold eddy on  
13   phytoplankton production and assemblage in Luzon Strait bordering the South China Sea,  
14   *J.Oceanogr*, *63*, 671-683, doi:10.1007/s10872-007-0059-9, 2007.
- 15   Chi, P.C., Chen, Y., and Lu, S.: Wind-driven South China Sea deep basin warm-core/cold  
16   eddies, *J.Oceanogr*, *54*, 347-360, doi:10.1007/BF02742619, 1998.
- 17   Cloern, J.E., Grenz, C., and Vidergar-Lucas, L.: An empirical model of the phytoplankton  
18   chlorophyll: carbon ratio-the conversion factor between productivity and growth rate. *Limnol.*  
19   *Oceanogr.*, *40*, 1313-1321, 1995.
- 20   Evans, G.T., and J.S.Parslow, A model of annual plankton cycles, *Biol. Oceanogr.*, **3**,  
21   328-347, 1985.
- 22   Fang, G., Chen, H., Wei, Z., Wang, Y., Wang, X., and Li, C.: Trends and interannual  
23   variability of the South China Sea surface winds, surface height, and surface temperature in  
24   the recent decade, *J. Geophys. Res.*, *111*, C11S16, doi:10.1029/2005JC003276, 2006.
- 25   Fasham, M.J.R., Variations in the seasonal cycle of biological production in subarctic oceans:  
26   A model sensitivity analysis, *Deep Sea Res. I*, **42**, 1111-1149, 1995.
- 27   Gan, J., and Qu, T.: Coastal jet separation and associated flow variability in the southwest  
28   South China Sea, *Deep Sea Res., Part I*, *55(1)*, 1-19, doi:10.1016/j.dsr.2007.09.008, 2008.
- 29   Hu, J., Kawamura, H., Hong, H., and Qi, Y.: A review on the currents in the South China Sea:  
30   Seasonal circulation, South China Sea warm current and Kuroshio intrusion, *J.Oceanogr*, *56*,  
31   607-624, 2000.

- 1 Hurtt, G.C., and R.A. Armstrong, A pelagic ecosystem model calibrated with BATS  
2 data, *Deep Sea Res. II*, **43**, 653-683, 1996.
- 3 Kalnay, E., Kanamitsu, M., Kistler, R. et al.: The NCEP/NCAR 40-year reanalysis project,  
4 *Bull. Am. Meteorol. Soc.*, **77**, 437-471, 1996.
- 5 Kuo, N.J., Zheng, Q.A., and Ho, C.B.: Satellite observation of upwelling along the western  
6 coast of the South China Sea, *Remote Sens. Environ.*, **74**, 463-470, 2000.
- 7 Kuo, N.J., Zheng, Q.A., and Ho, C.B.: Response of Vietnam coastal upwelling to the  
8 1997-1998 ENSO event observed by multisensory data, *Remote Sens. Environm.*, **89**, 106-115,  
9 2004.
- 10 Li, L., Nowlin, Jr., W.D., and Jilan, S.: Anticyclonic rings from the Kuroshio in the South  
11 China Sea, *Deep-Sea Res., I*, **45**, 1469-1482, 1998.
- 12 Lin, I.-I., Lien, C.-C., Wu, C.-R., Wong, G.T.F., Huang, C.-W., and Chiang, T.-L.: Enhanced  
13 primary production in the oligotrophic South China Sea by eddy injection in spring, *Geophys.*  
14 *Res. Lett.*, **37**, L16602, doi:10.1029/2010GL043872, 2010.
- 15 Liu, G. and Chai, F.: Seasonal and interannual variability of primary and export production in  
16 the South China Sea: a three-dimensional physical-biogeochemical model study, *ICES J. Mar.*  
17 *Sci.*, **66**(2), 420-431, doi:10.1093/icesjms/fsn219, 2009.
- 18 Liu, K.K., Chao, S.Y., Shaw, P.T., Gong, G.C., Chen, C.C., and Tang, T.Y.: Monsoon-forced  
19 chlorophyll distribution and primary production in the South China Sea: observations and a  
20 numerical study, *Deep-Sea Res. I*, **49**, 1387-1412, 2002.
- 21 Liu, K.K., Chen, Y.J., Tseng, C.M., Lin, I.I., Liu, H.B., and Snidvongs, A.: The significance  
22 of phytoplankton photo-adaptation and benthic-pelagic coupling to primary production in the  
23 South China Sea: Observations and numerical investigations, *Deep-Sea Res. II*, **54**,  
24 1546-1574, 2007.
- 25 Liu, Q., Jiang, X., Xie, S.-P., and Liu, T.: A gap in the Indo-Pacific warm pool over the South  
26 China Sea in boreal winter: Seasonal development and interannual variability, *J. Geophys.*  
27 *Res.*, **109**, C07012, doi:10.1029/2003JC002179, 2004.
- 28 Liu, Q., Kaneko, A., and Jilan, S.: Recent progress in studies of the South China Sea  
29 circulation, *J. Oceanogr.*, **64**(5), 753-762, doi:10.1007/s10872-008-0063-8, 2008.
- 30 Liu, W.T., and Xie, X.: Space-based observations of the seasonal changes of the South Asian

1 Monsoons and oceanic response, *Geophys. Res. Lett.*, 26, 1473-1476,  
2 doi:10.1029/1999GL900289, 1999.

3 Liu, X., Wang, J., Cheng, X., and Du, Y.: Abnormal upwelling and chlorophyll-a  
4 concentration off South Vietnam in summer 2007, *J. Geophys. Res.*, 117, C07021,  
5 doi:10.1029/2012JC008052, 2012.

6 Masumoto, Y., Sasaki, H., Kagimoto, T., Komori, N., Ishida, A., Sasai, Y., Miyama, T.,  
7 Motoi, T., Mitsudera, H., Takahashi, K., and Sakuma, H.: A fifty-year-eddy-resolving  
8 simulation of the world ocean: Preliminary outcomes of OFES (OGCM for the Earth  
9 Simulator), *J. Earth Simulator*, 1, 35-56, 2004.

10 Ning, X., Chai, F., Xue, H., Cai, Y., Liu, C., and Shi, J.: Physical-biological oceanographic  
11 coupling influencing phytoplankton and primary production in the South China Sea, *J.*  
12 *Geophys. Res.*, 109, C10005, doi:10.1029/2004JC002365, 2004.

13 Oschlies, A.: Model-derived estimates of new production: New results point towards lower  
14 values, *Deep-Sea Res. II*, 48, 2173-2197, 2001.

15 Pacanowski, R.C., and Griffies, S.M.: *MOM 3.0 Manual*, Geophysical Fluid Dynamics  
16 Laboratory/National Oceanic and Atmospheric Administration, 680pp, 2000.

17 Qu, T.: Upper-layer circulation in the South China Sea, *J. Phys. Oceanogr.*, 30, 1450-1460,  
18 2000.

19 Qu, T., Mitsudera, H., and Yamagata, T.: Intrusion of the North Pacific waters into the South  
20 China Sea, *J. Geophys. Res.*, 15, 6415-6424, 2000.

21 Saji, N.H., Goswami, B.N., Vinayachandran, P.N., and Yamagata, T.: A dipole mode in the  
22 tropical Indian Ocean, *Nature*, 401:360-363, 1999.

23 Sarmiento, J.L., R.D. Slater, M.J.R. Fasham, H.W. Ducklow, J.R. Toggweiler, and G.T. Evans,  
24 A seasonal three-dimensional ecosystem model of nitrogen cycling in the North Atlantic  
25 euphotic zone, *Global Biogeochem. Cycles*, 7, 417-450, 1993.

26 Sasai, Y., Ishida, A., Sasaki, H., Kawahara, S., Uehara, H., and Yamanaka, Y.: A global  
27 eddy-resolving coupled physical and biological model: Physical influences on a marine  
28 ecosystem in the North Pacific, *Simulation*, 82, 467-474, 2006.

29 Sasai, Y., Richards, K.J., Ishida, A., and Sasaki, H.: Effects of cyclonic mesoscale eddies on  
30 the marine ecosystem in the Kuroshio Extension region using an eddy-resolving coupled

- 1 physical-biological model, *Ocean Dynamics*, doi:10.1007/s10236-010-0264-8, 60(3), 693-704,  
2 2010.
- 3 Shaw, P.T. and Chao, S.Y.: Surface circulation in the South China Sea, *Deep-Sea Res. I*, 41,  
4 1663-1683, 1994.
- 5 Tang, D.L., Ni, I.H., Kestner, D.R., and Müller-Kargen, F.E.: Remote sensing observations of  
6 winter phytoplankton blooms southeast of the Luzon Strait in the South China Sea, *Mar. Ecol.*  
7 *Prog. Ser.*, 191, 43-51, 1999.
- 8 Tang, D.L., Kawamura, H., Dien, T.V., and Lee, M.A.: Offshore phytoplankton biomass  
9 increase and its oceanographic causes in the South China Sea, *Mar. Ecol. Prog. Ser.*, 268,  
10 31-41, 2004.
- 11 Wang, L.P., Koblinsky, C.J., and Howden.: Mesoscale variability in the South China Sea  
12 from the TOPEX/POSEIDON altimetry data, *Deep Sea Res., Part I*, 47(4), 681-708,  
13 doi:10.1016/S0967-0637(99)00068-0,2000
- 14 Wang, G., Su, J., and Chu, P.C.: Mesoscale eddies in the South China Sea detected from the  
15 altimeter data, *Geophys. Res. Lett.*, 30(21), 2121, doi:10.1029/2003GL018532, 2003.
- 16 Wang, J.J., Tang, D.L., and Sui, Y.: Winter phytoplankton bloom induced by subsurface  
17 upwelling and mixed layer entrainment southwest of Luzon Strait, *J. Mar. Systems*, 83,  
18 141-149, 2010.
- 19 Wyrтки, K.: Physical oceanography of the south-east Asian waters. NAGA Report Vol. 2,  
20 Scientific Results of Marine Investigations of the South China Sea and the Gulf of Thailand.  
21 Scripps Institution of Oceanography, La Jolla, CA, 195pp, 1961.
- 22 Xie, S.-P., Xie, Q., Wang, D., and Liu, W.T.: Summer upwelling in the South China Sea and  
23 its role in regional climate variations, *J. Geophys. Res.*, 108(C8), 3261,  
24 doi:10.1029/2003JC001867, 2003.
- 25 Xiu, P., Chai, F., Shi, L., Xue, H., and Chao, Y.: A census of eddy activities in the South  
26 China Sea during 1993-2007, *J. Geophys. Res.*, 115, C03012, doi:10.1029/2009JC005657,  
27 2010.
- 28 Xiu, P., and Chai, F.: Modeled biogeochemical responses to mesoscale eddies in the South  
29 China Sea, *J. Geophys. Res.*, 116, C10006, doi:10.1029/2010JC006800, 2011.
- 30 Yang, H.J., and Liu, Q.Y.: Forced Rossby wave in the northern South China Sea, *Deep Sea*

- 1 *Res., Part I, 50(7)*, 917-926, doi:10.1016/S0967-0637(03)00074-8,2003.
- 2 Yang, J.L., Liu Q.Y., and Liu, Z.Y.: Linking observations of the Asian monsoon to the Indian  
3 Ocean SST: Possible roles of Indian Ocean basin mode and dipole mode, *J. Clim.*, *23(21)*,  
4 5889-5902, doi:10.1175/2010JC12962.1, 2010.
- 5 Zhuang, W., Xie, S.-P., Wand, D., Taguchi, B., Aiki, N, and Sasaki, H.: Interseasonal  
6 variability in sea surface height over the South China Sea, *J. Geophys. Res.*, *115*, C04010,  
7 doi:10.1029/2009JC005647, 2010.

8

9

## 10 **Figure captions**

11 Figure 1. Climatological monthly mean surface chlorophyll concentration ( $\text{mg m}^{-3}$ ) during  
12 2000-2007 from (a) SeaWiFS and (b) OFES, (c) vertical mean nitrate concentration ( $\text{mmol N}$   
13  $\text{m}^{-3}$ ) upper 73 m depth with thermocline depth (contour in m,  $20^\circ\text{C}$  isotherm depth), and (d)  
14 vertical nitrate flux ( $\text{mmol N m}^{-2} \text{day}^{-1}$ ) at 73 m depth in OFES. Boxes off northwestern  
15 Luzon, and southeast Vietnam are upwelling regions (L and V) discussed in the text. Positive  
16 nitrate flux is upward. Negative nitrate flux is opposite sign.

17

18 Figure 2. Climatological monthly mean sea surface height anomaly (cm) during 2000-2007  
19 from (a) AVISO and (b) OFES, (c) eddy kinetic energy ( $\text{cm}^2 \text{s}^{-2}$ ) in the surface layer, and (d)  
20 Ekman pumping ( $\times 10^{-6} \text{m s}^{-1}$ ) with wind stress ( $\text{N m}^{-2}$ ) in OFES. Contour line in (a) and (b) is  
21 0 cm. AVISO is Archiving, Validation, and Interpretation of Satellite Oceanographic data  
22 altimeter products.

23

24 Figure 3. Time series of climatological monthly mean surface chlorophyll concentrations,  
25 thermocline depth, vertical mean nitrate concentration, and vertical nitrate flux at 73 m depth  
26 averaged for each upwelling region of Fig. 1: (a) Box-L of northwestern Luzon ( $16^\circ\text{N}$ - $20^\circ\text{N}$ ,  
27  $116^\circ\text{E}$ - $120^\circ\text{E}$ ) and (b) Box-V of southeast Vietnam ( $11^\circ\text{N}$ - $15^\circ\text{N}$ ,  $110^\circ\text{E}$ - $114^\circ\text{E}$ ). Mean surface  
28 chlorophyll concentration  $\pm$  standard deviation, and correlation coefficient ( $r$ ) are also  
29 presented for each box.

1

2 Figure 4. Time series of monthly mean surface chlorophyll concentrations ( $\text{mg m}^{-3}$ ) and wind  
3 stress ( $\text{N m}^{-2}$ ) averaged for each upwelling region of Fig. 1 during 2000-2007 in (a)-(b) Box-L  
4 and (c)-(d) Box-V. Mean surface chlorophyll concentration  $\pm$  standard deviation, and  
5 correlation coefficient ( $r$ ) are also presented for each box.

6

7 Figure 5. Time series of simulated vertical distribution of (a) chlorophyll concentration ( $\text{mg}$   
8  $\text{m}^{-3}$ ) with nutricline depth ( $1 \text{ mmol N m}^{-3}$ , dashed line) and thermocline depth ( $20^\circ\text{C}$ , solid  
9 line), (b) nitrate concentration ( $\text{mmol N m}^{-3}$ ) with potential density (dashed line), (c)  
10 temperature ( $^\circ\text{C}$ ) with mixed layer depth (dashed line), and (d) vertical velocity ( $\text{m day}^{-1}$ )  
11 averaged for Box-L (northwestern Luzon, L in Fig. 1) during 2000-2007.

12

13 Figure 6. Same as for Fig. 5, but for Box-V (southeast Vietnam, V in Fig. 1).

14

15 Figure 7. Distribution of sea surface height anomaly (cm) of (a) 20 cm and (b) -20cm during  
16 2000-2007 from OFES. Positive anomaly denotes anticyclonic eddy. Negative anomaly  
17 denotes cyclonic eddy.

18

19 Figure 8. Snapshots of simulated (a) sea surface height anomaly (color, cm) and surface  
20 horizontal velocity (vectors,  $\text{cm s}^{-1}$ ), (b) surface chlorophyll concentration ( $\text{mg m}^{-3}$ ), (c)  
21 nitrate concentration at 73 m depth ( $\text{mmol N m}^{-3}$ ), and (d) vertical velocity at 78 m depth ( $\text{m}$   
22  $\text{day}^{-1}$ ) from November 2003 to February 2004 in the northeastern South China Sea. Dashed  
23 line in (d) is the center of anticyclonic eddy location.

24

25 Figure 9. Vertical distribution of snapshots of simulated (a) chlorophyll concentration ( $\text{mg}$   
26  $\text{m}^{-3}$ ), (b) nitrate concentration (color,  $\text{mmol N m}^{-3}$ ) and potential density (contour), and (c)  
27 vertical velocity ( $\text{m day}^{-1}$ ) from November 2003 to February 2004 along the center of  
28 anticyclonic eddy (dashed line in Fig. 8d). Contour interval in (b) is 0.2.

29

1 Figure 10. Snapshots of simulated surface chlorophyll concentration (color,  $\text{mg m}^{-3}$ ) and  
 2 surface horizontal velocity (vectors,  $\text{cm s}^{-1}$ ) in the northeastern South China Sea: (a) January,  
 3 16, 2002, (b) January, 16, 2006, and (c) January, 14, 2007.

4

5 Figure 11. Snapshots of simulated (a) sea surface height anomaly (color, cm) and surface  
 6 horizontal velocity (vectors,  $\text{cm s}^{-1}$ ), (b) surface chlorophyll concentration ( $\text{mg m}^{-3}$ ), (c)  
 7 nitrate concentration at 73 m depth ( $\text{mmol N m}^{-3}$ ), and (d) vertical velocity at 78 m depth ( $\text{m}$   
 8  $\text{day}^{-1}$ ) from June 2002 to September 2002 in the southwestern South China Sea.

9

10 Figure 12. Vertical distribution of snapshots of simulated (a) chlorophyll concentration ( $\text{mg}$   
 11  $\text{m}^{-3}$ ), (b) nitrate concentration (color,  $\text{mmol N m}^{-3}$ ) and potential density (contour), and (c)  
 12 vertical velocity ( $\text{m day}^{-1}$ ) from June 2002 to September 2002 along  $111^\circ\text{E}$  in the  
 13 southwestern South China Sea. Contour interval in (b) is 0.2.

14

15

16 Table A1. Parameters of ecosystem model

17

Parameter	Symbol	Value	Units
<i>Phytoplankton (P) Coefficients</i>			
Integration method for daily growth rate		<i>Evans and Parslow</i> [1985]	
Half saturation constant for N uptake	$k_I$	0.5	$\text{mmol m}^{-3}$
Specific mortality/recycling rate	$\mu_P$	0.05	$\text{day}^{-1}$
Quadratic mortality rate	$\mu_{PP}$	0.05	$(\text{mmol m}^{-3})^{-1} \text{d}^{-1}$
<i>Zooplankton (Z) Coefficients</i>			
Assimilation efficiency	$\gamma_1$	0.75	
Maximum grazing rate	$g$	2.0	$\text{day}^{-1}$
Prey capture rate	$\epsilon$	1.0	$(\text{mmol m}^{-3})^{-2} \text{d}^{-1}$
(Quadratic) mortality	$\mu_Z$	0.20	$(\text{mmol m}^{-3})^{-1} \text{d}^{-1}$
Excretion	$\gamma_2$	0.03	$\text{day}^{-1}$
<i>Detritus (D) Coefficients</i>			
Remineralization rate	$\mu_D$	0.05	$\text{day}^{-1}$
Sinking velocity	$w_S$	5.0	$\text{m d}^{-1}$

18

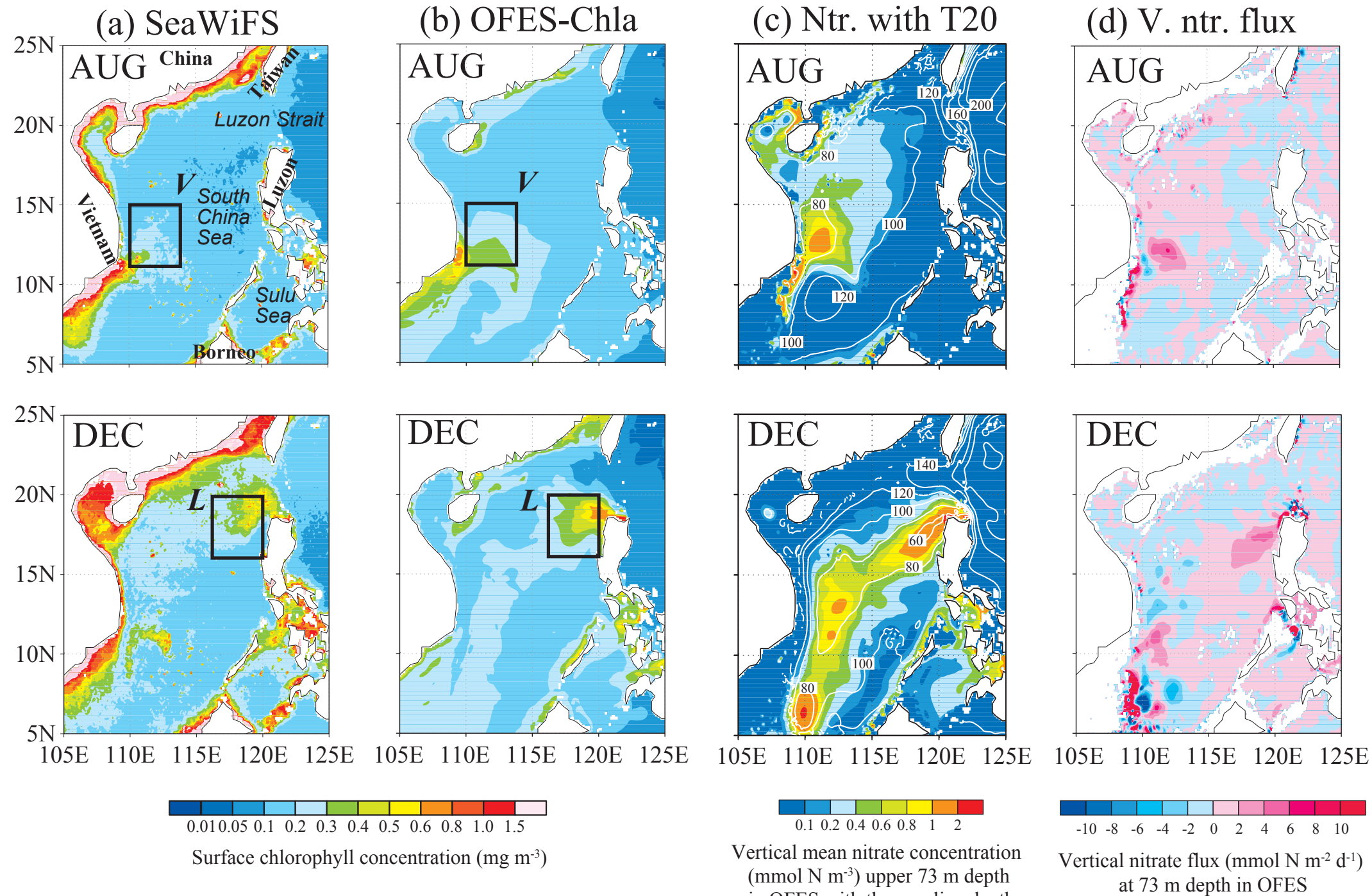


Figure 1.

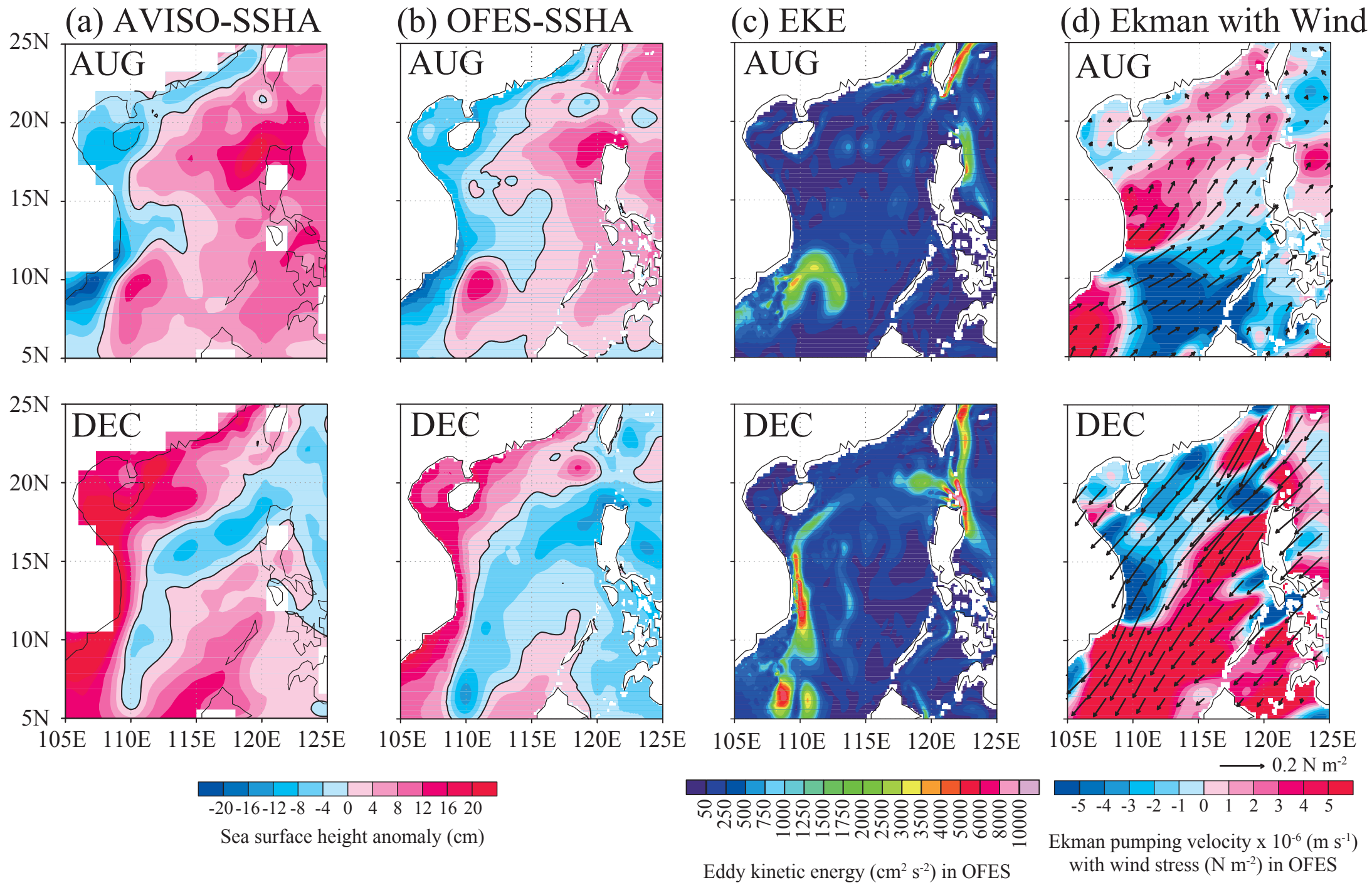


Figure 2.

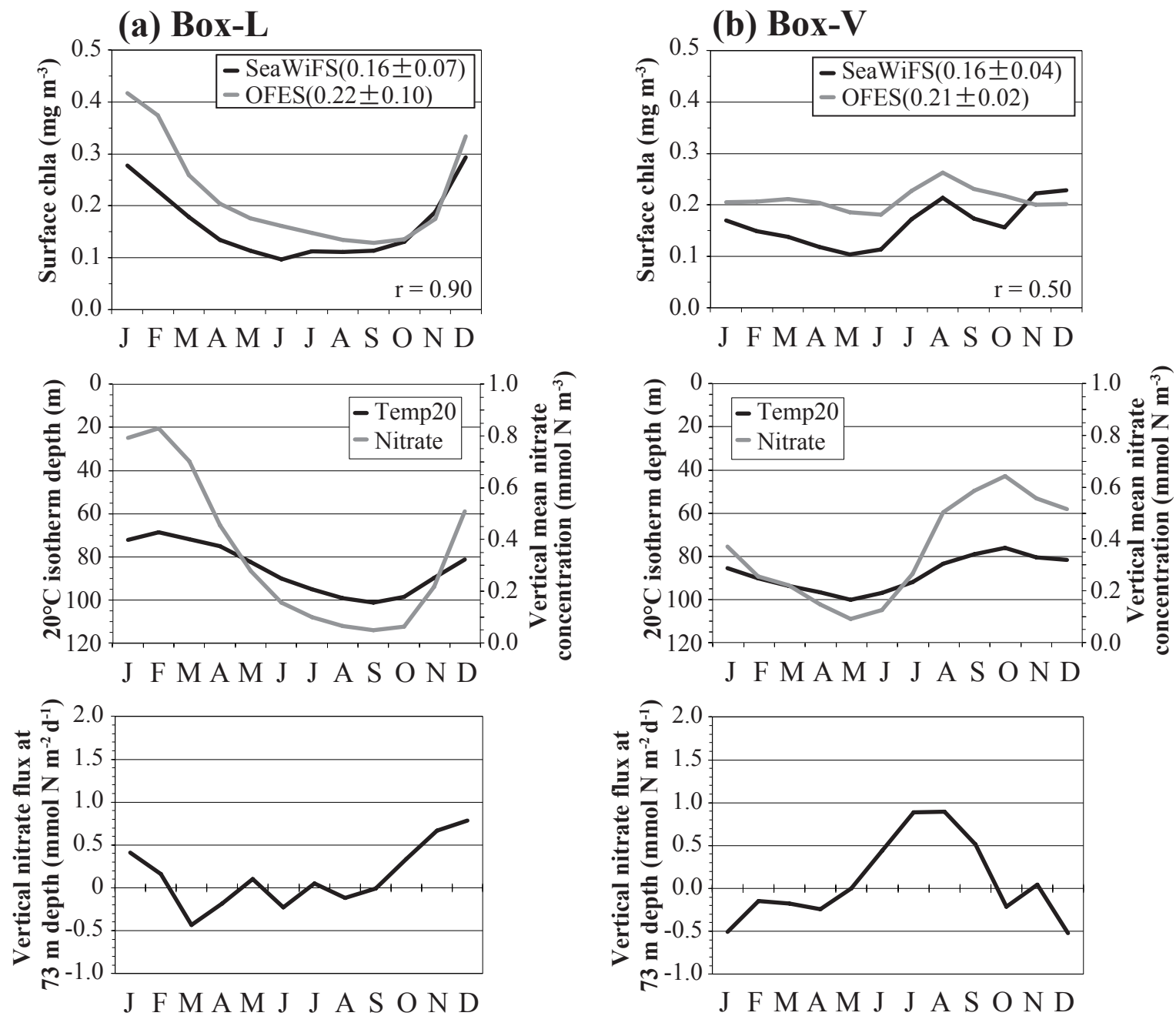


Figure 3.

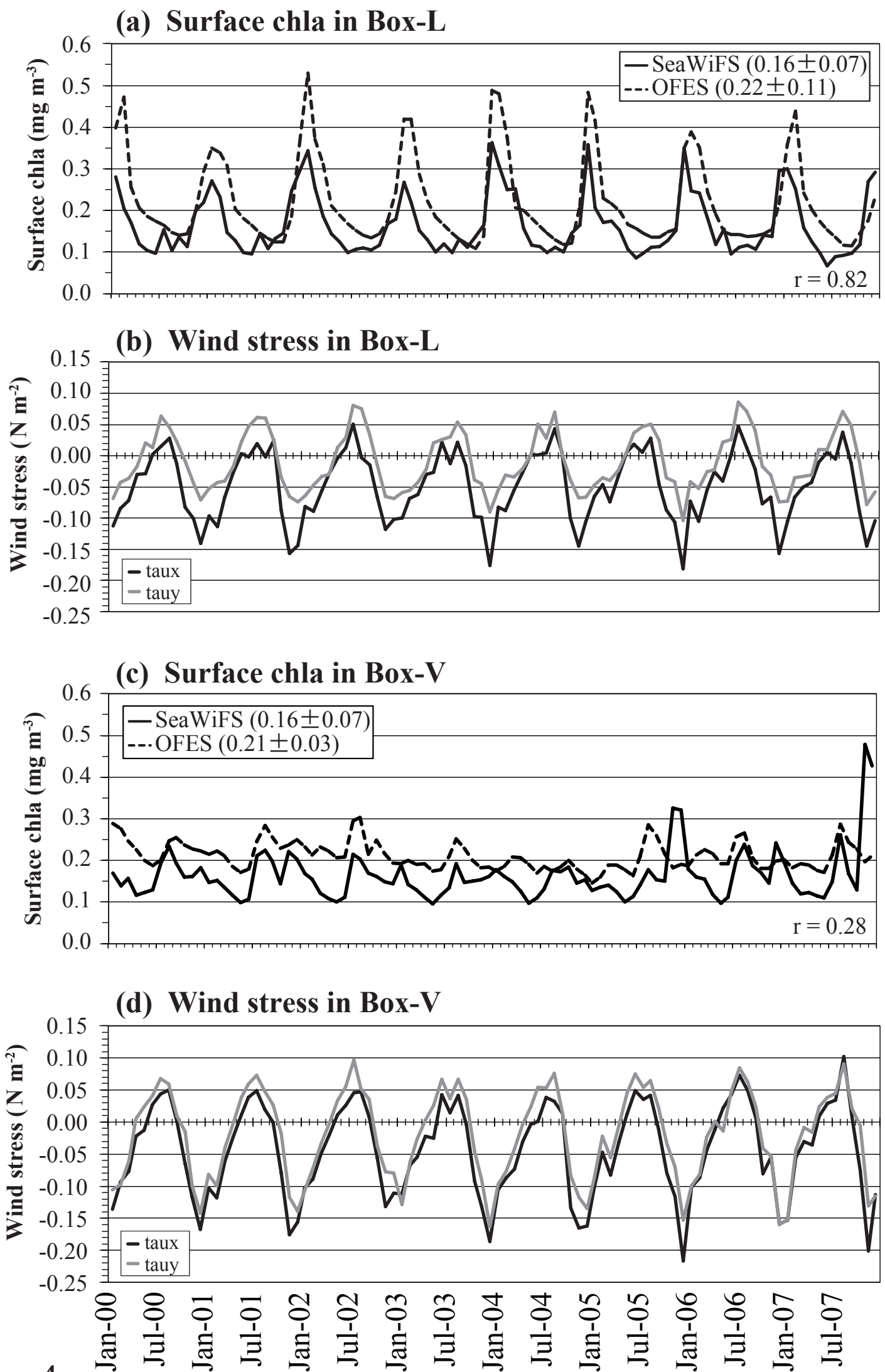
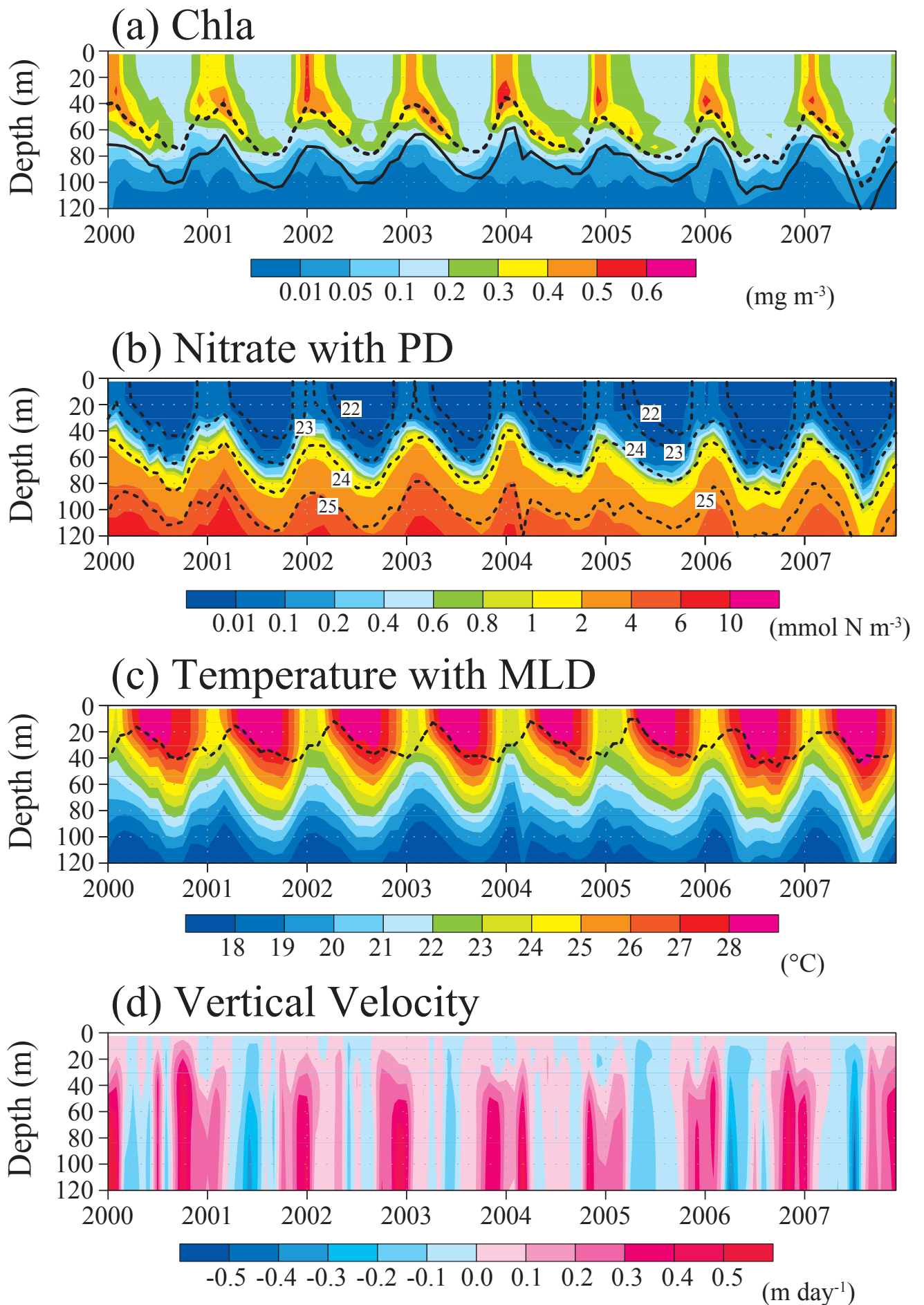
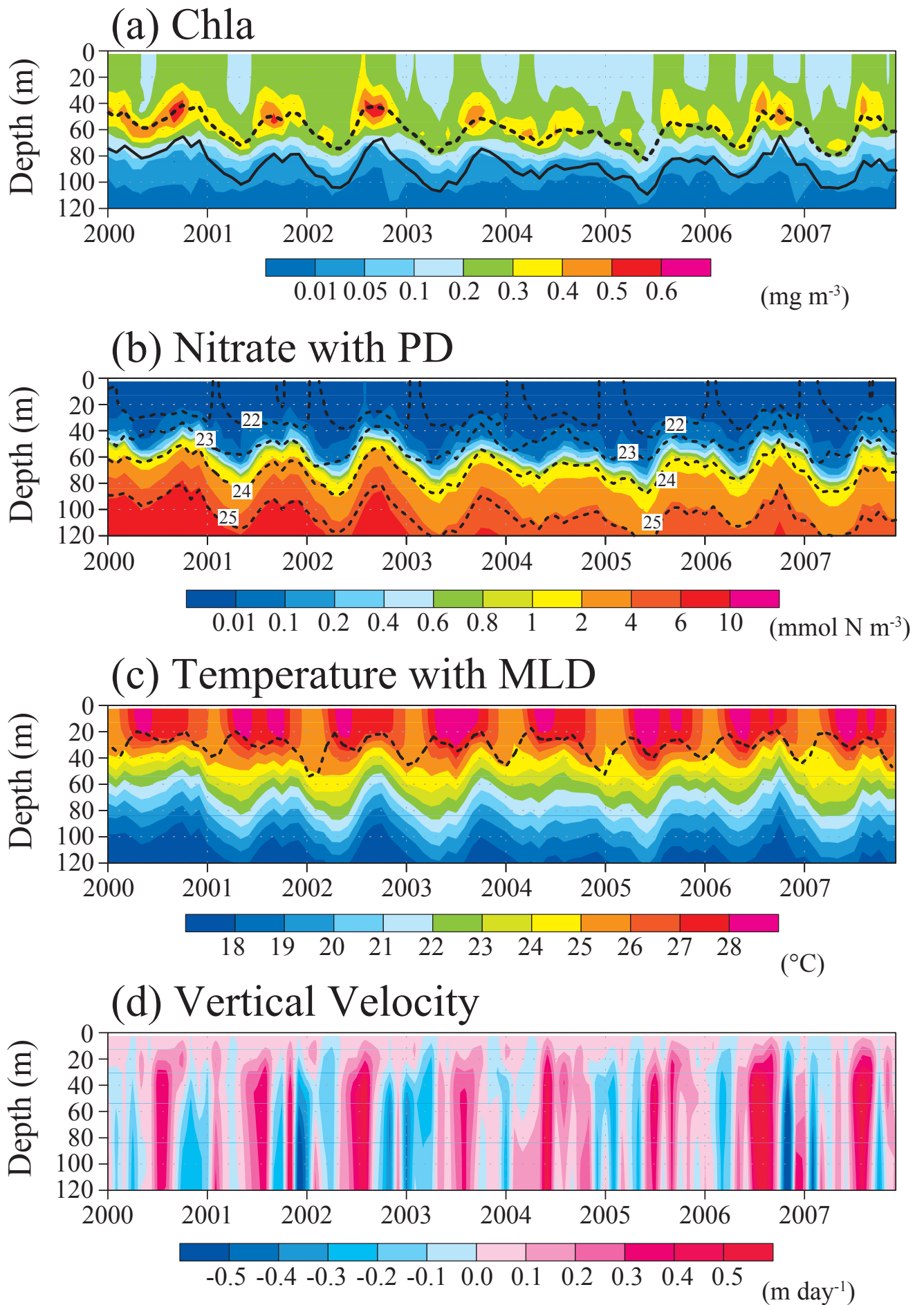


Figure 4.



**Box-L (16°N-20°N, 116°E-120°E)**

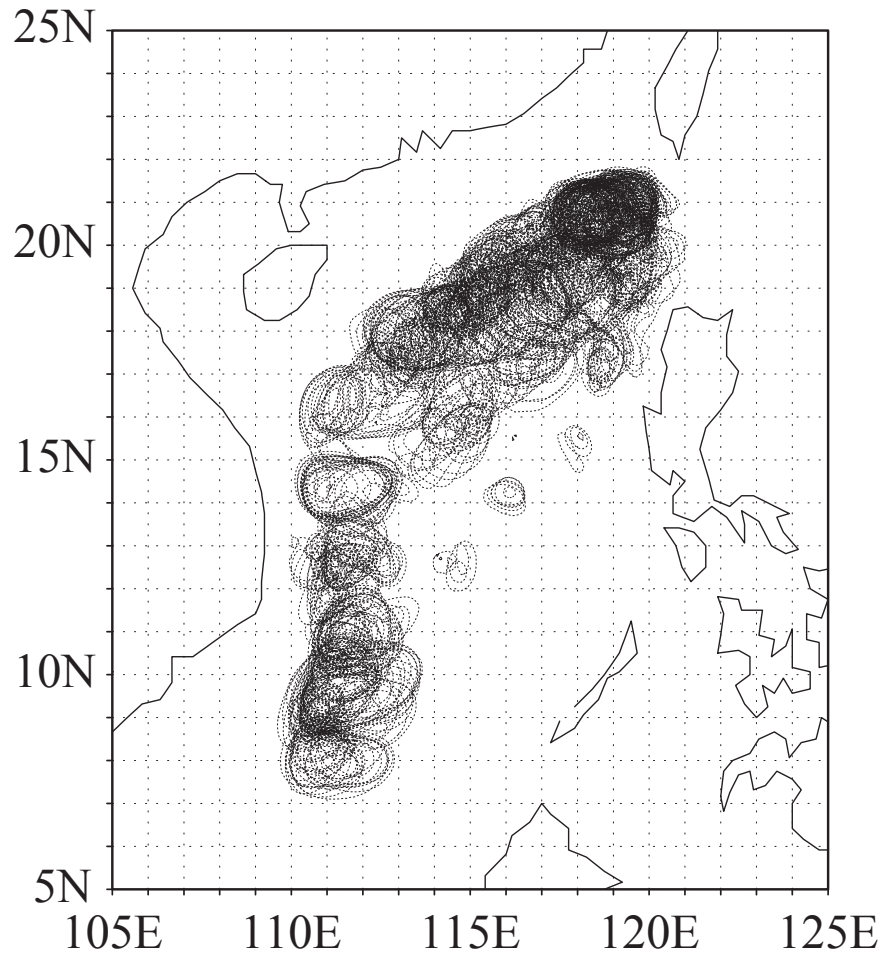
Figure 5.



**Box-V (11°N-15°N, 110°E-114°E)**

Figure 6.

(a) SSHA 20cm contours during 2000-2007



(b) SSHA -20cm contours during 2000-2007

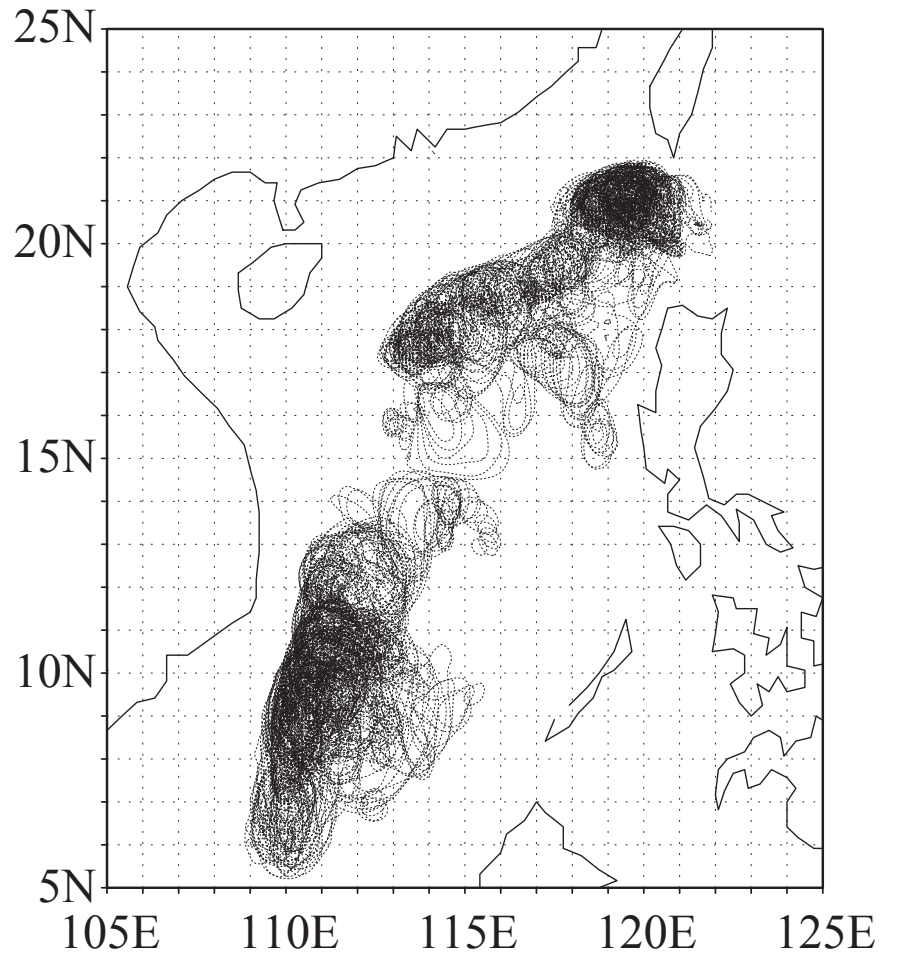
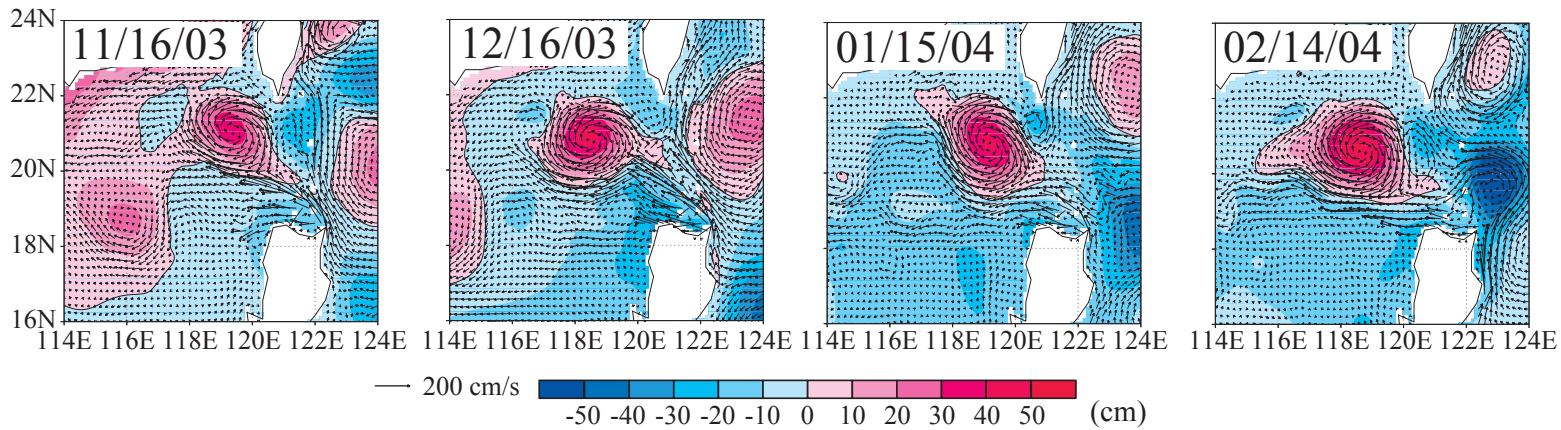
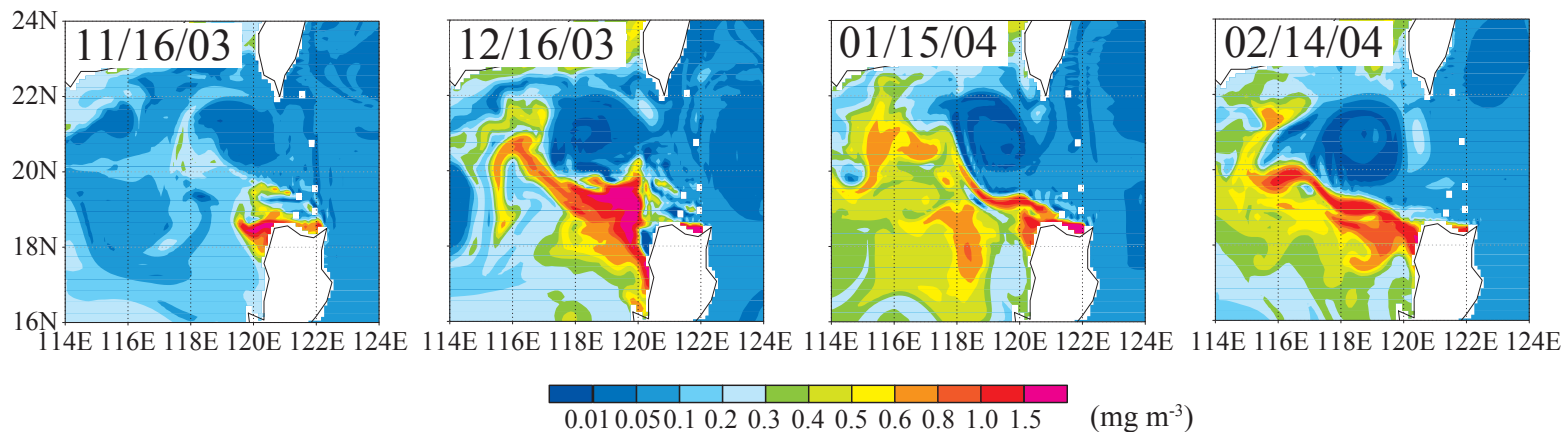


Figure 7.

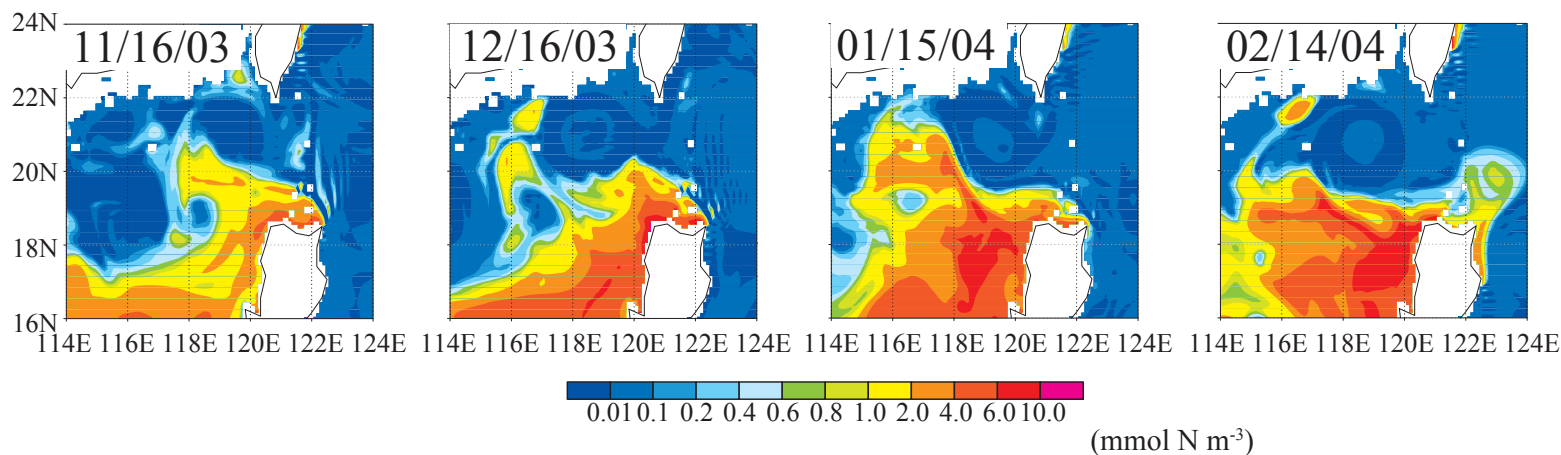
### (a) SSHA with surface H-Vel.



### (b) Surface chla



### (c) Nitrate concentration at 73 m depth



### (d) Vertical velocity at 78 m depth

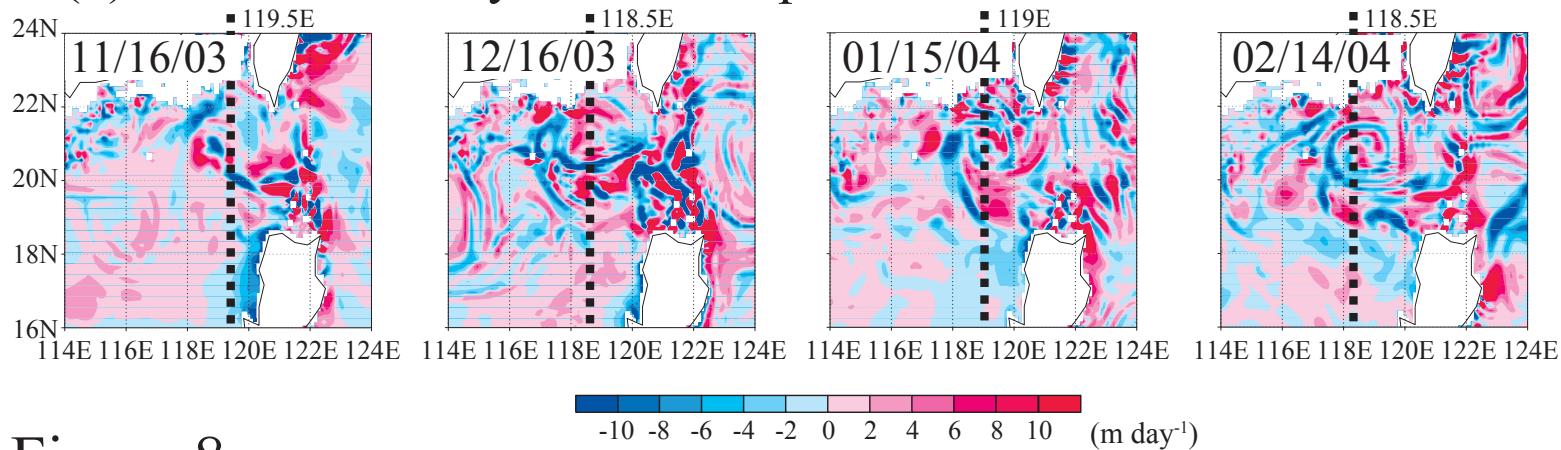


Figure 8.

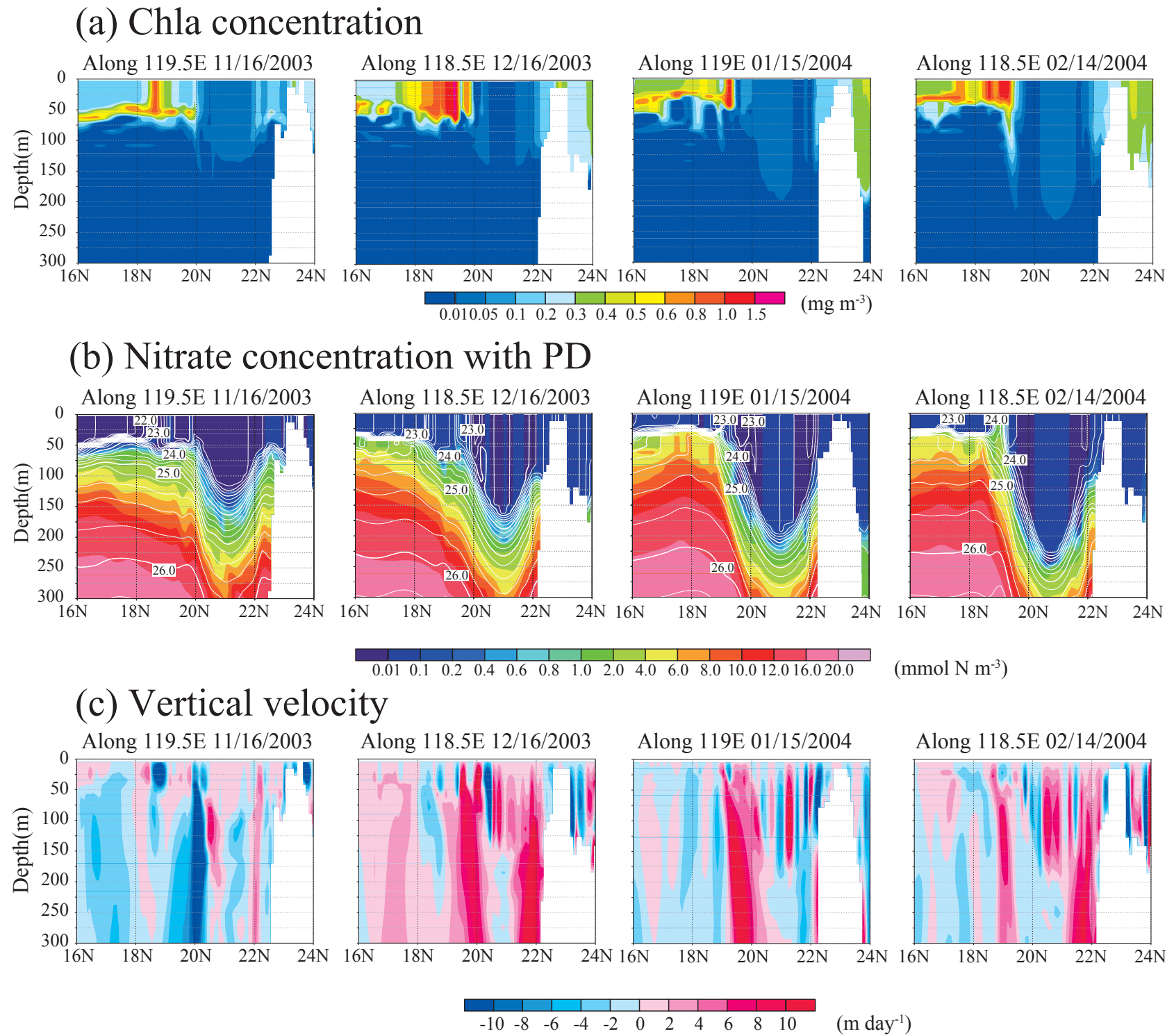


Figure 9.

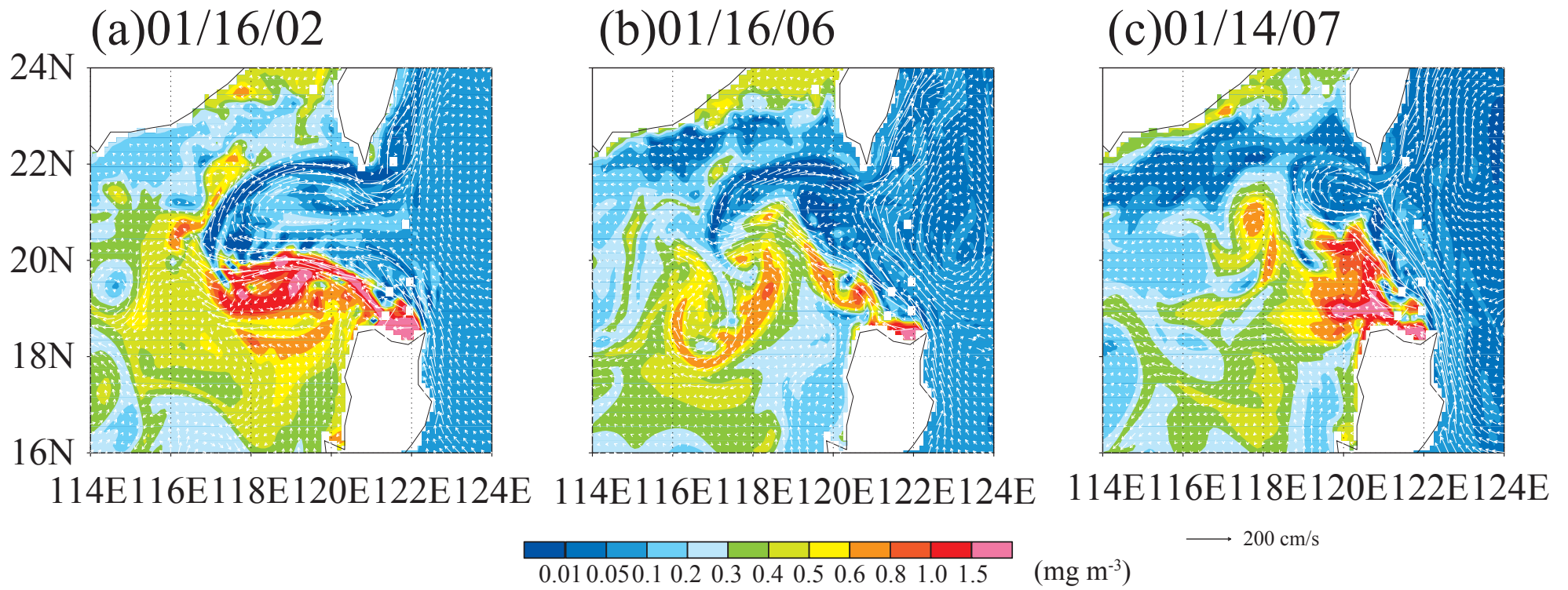
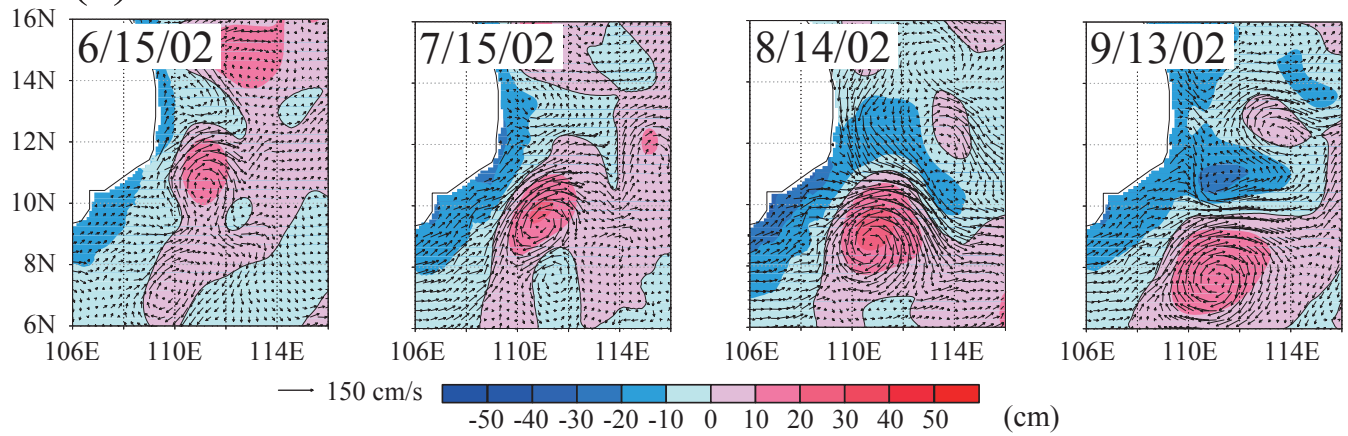
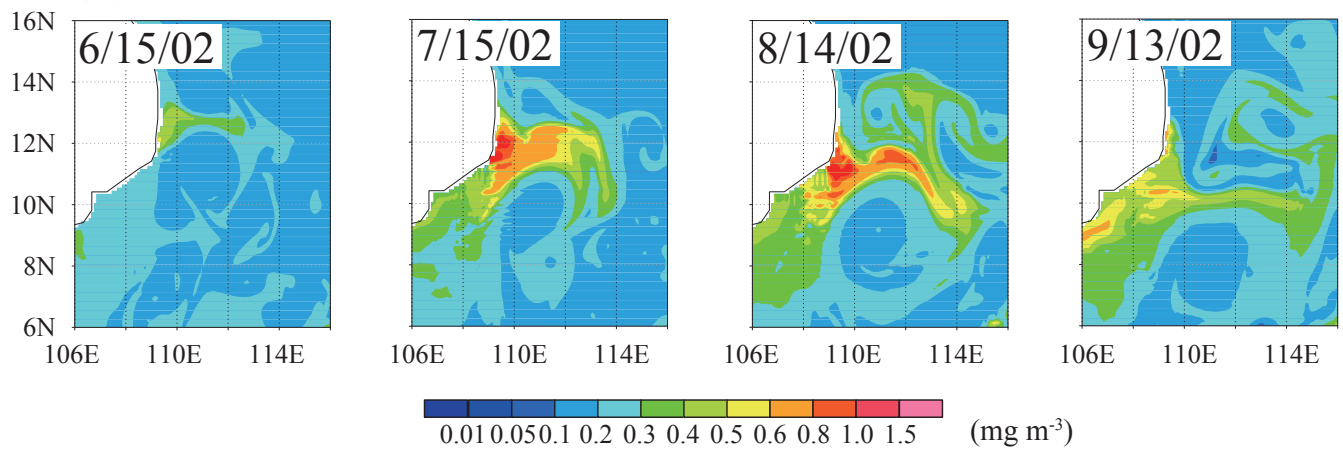


Figure 10.

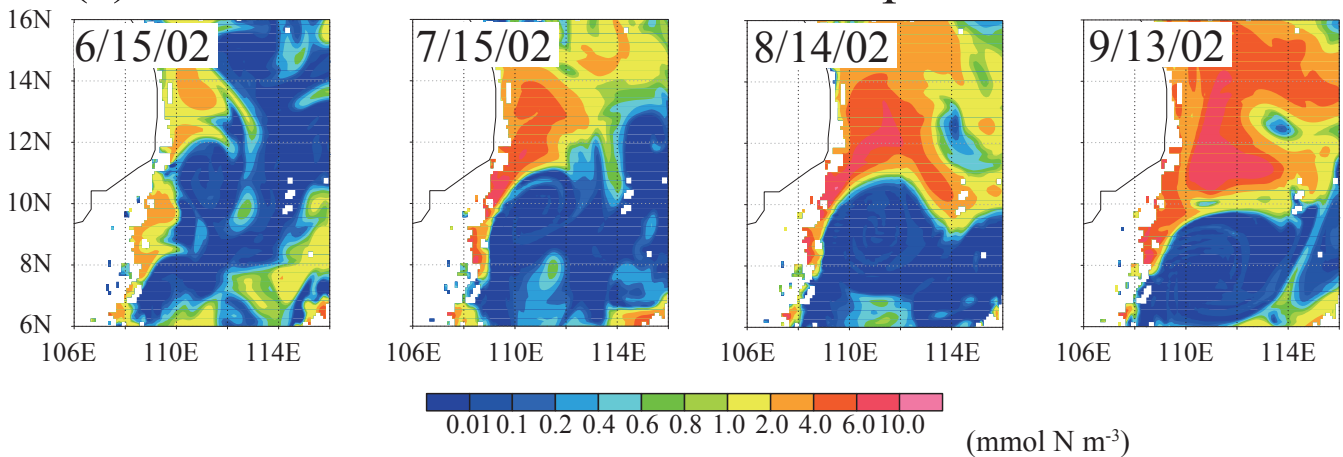
(a) SSHA with surface H-Vel.



(b) Surface chla



(c) Nitrate concentration at 73 m depth



(d) Vertical velocity at 78 m depth

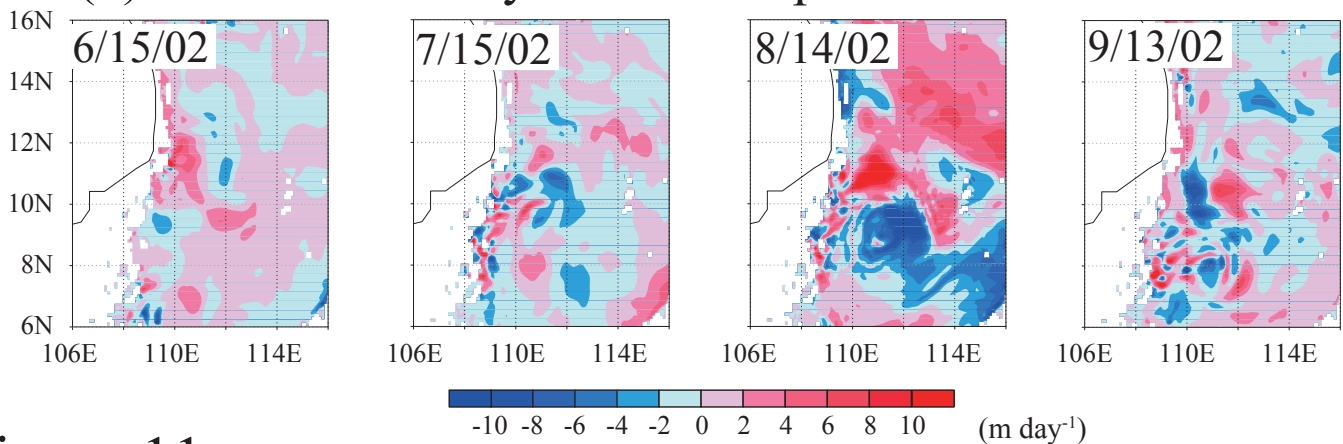
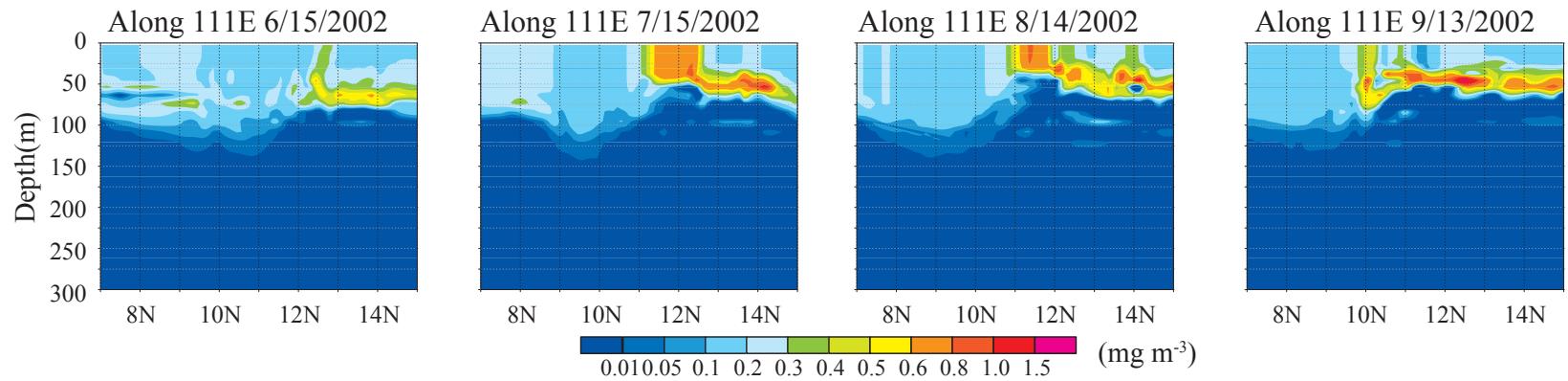
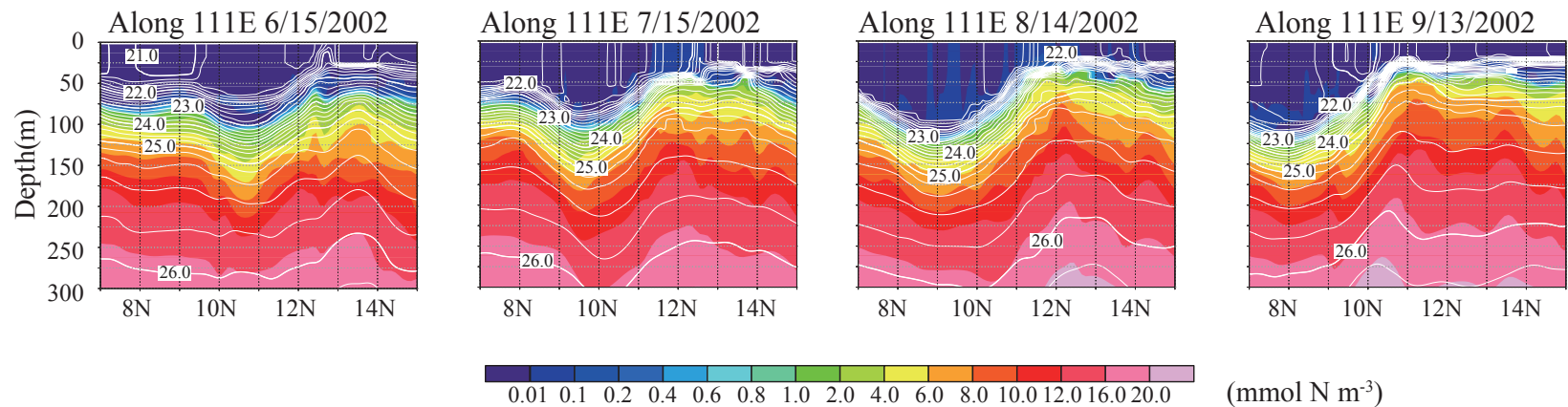


Figure 11.

### (a) Chla concentration



### (b) Nitrate concentration with PD



### (c) Vertical velocity

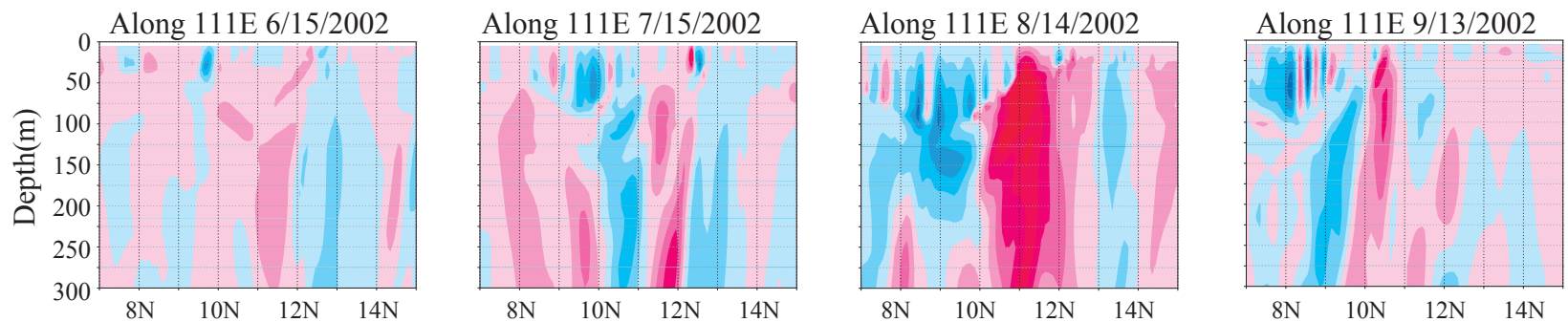


Figure 12.